THE GEOLOGICAL SOCIETY
OF AMERICA®

Tectonically controlled drainage fragmentation in the southwestern Great Basin, USA

B.M. Lutz[1,†], J.R. Knott[2], F.M. Phillips[1], M.T. Heizler[3], K.A. Heitkamp, Jr.[2,§], E.L. Griffie[2,#], G.A. Axen[1], and J.P. Calzia[4]

[1]*Earth and Environmental Science Department, New Mexico Institute of Mining and Technology, 801 Leroy Place, Socorro, New Mexico 87801, USA*
[2]*Department of Geological Sciences, California State University-Fullerton, 800 North State College Boulevard, Fullerton, California 92834, USA*
[3]*Geochronology Research Laboratories, New Mexico Bureau of Geology and Mineral Resources, 801 Leroy Place, Socorro, New Mexico 87801, USA*
[4]*U.S. Geological Survey, 345 Middlefield Road, Menlo Park, California 94025, USA*

ABSTRACT

The area now occupied by the Great Basin, western USA, contained paleo-fluvial systems that predated the modern-day endorheic (closed) basins. The areal extent of these paleo-fluvial systems within the southwestern Great Basin is known mainly from isolated remnants preserved in the modern mountain ranges. We document the age, extent, and tectonic disruption of Mio-Pliocene fluvial systems of the southwestern Great Basin. Synthesis of new field observations, geochemistry, and geochronology with existing studies defines two latest Miocene to Pliocene east-southeast flowing drainages that predated the modern endorheic basins. The drainage network was ultimately fragmented in Pliocene time (ca. 3.5-4 Ma). Fragmentation of the drainage network led to lake formation, drying of lakes, and the formation of isolated springs. The rapid environmental changes initiated by faulting and volcanism isolated previously interbreeding populations of spring-dwelling taxa and have caused divergent evolution since Pliocene time. Modern endemism within the region's springs is thus a direct consequence of intraplate tectonism.

[†]Present address: Geosciences and Environmental Change Science Center, U.S. Geological Survey, Denver Federal Center, Lakewood, Colorado 80215, USA; blutz@usgs.gov.
[§]Present address: Arcadis of Michigan, LLC, 28550 Cabot Drive, Suite, 500, Novi, Michigan 48377, USA.
[#]Present address: ENGEO, Inc., 320 Goddard Way, Suite 100, Irvine, California 92618, USA.

INTRODUCTION

Faulting and volcanism can produce mountain ranges that alter regional hydrological and ecological systems (Craw et al., 2008; Luebert and Muller, 2015; Antonelli et al., 2018; Rahbek et al., 2019; Perrigo et al., 2020). The Great Basin of the western USA represents a prime example of such interplay. Dozens of endorheic (internally drained) basins are separated by fault-bounded mountain ranges. The 300–800-km-wide physiographic province formed from a pre-existing high elevation, low-relief plateau that spanned much of the southwestern USA Cordillera from Paleocene to middle Eocene time (e.g., Coney and Harms, 1984; DeCelles, 2004; Cassel et al., 2014; Chapman et al., 2020; Zhou and Liu, 2019).

This "Nevadaplano" (DeCelles, 2004) was capped by diachronous erosional surfaces crossed by paleo-channels that transported sediment for hundreds of kilometers (e.g., Busby and Putirka, 2009; Jayko, 2009; Henry et al., 2012; Busby et al., 2016; Miller et al., 2022). Extensional collapse from middle Eocene to Holocene time (e.g., McQuarrie and Wernicke, 2005; Zhou and Liu, 2019) eventually fragmented many fluvial links across the plateau, leaving the endorheic basins.

The southwestern Great Basin (Figs. 1 and 2) formed when a final remnant of the overthickened Nevadaplano crust extended and thinned (e.g., Dickinson, 2006). Most extension of the region was accomplished in late Miocene to Holocene times along regional detachment faults, range-bounding normal faults, and transtensional fault systems (Hamilton and Myers, 1966; Burchfiel and Stewart, 1966; Stewart, 1967, 1983; Wright et al., 1974; Wernicke et al., 1988; Lutz et al., 2021, 2022). The transtensional faults are part of the southern Walker Lane (see inset of Fig. 1). Extension and transtension in the area reduced local crustal thickness and average elevation from 50 km to 60 km and 2500–3500 m to 30–35 km and 1000–1500 m, respectively (e.g., Coney and Harms, 1984; Wernicke et al., 1988; Snow and Wernicke, 2000; Bahadori et al., 2018; Zhou and Liu, 2019; Lutz et al., 2021).

The young age of extension, well-studied faults, and preservation of pre-, syn-, and post-extensional sedimentary and volcanic rocks (e.g., Knott et al., 1999; Wright et al., 1999; Wernicke et al., 1988; Snow and Wernicke, 2000; Niemi et al., 2001; Fridrich and Thompson, 2011; Lutz et al., 2021) allow fairly precise paleogeographic reconstructions in the southwestern Great Basin (e.g., Snow and Wernicke, 2000; Fridrich and Thompson, 2011). However, most paleogeographic studies (Table 1) have focused on middle to late Miocene rocks.

Here, we constrain the age and extent of latest Miocene to Pliocene (ca. 6–3 Ma) drainage systems in the southwestern Great Basin by synthesizing new field observations, geochemistry, and geochronology with existing sedimentological studies. First, we review Miocene paleogeography and fluvio-lacustrine systems of the southwestern Great Basin area (Fig. 1 and Table 1). Then, we present new (1) field observations, (2) geochemical data, (3) paired detrital zircon U/Pb and detrital K-feldspar $^{40}Ar/^{39}Ar$ analyses of alluvial fanglomerates, and (4) $^{40}Ar/^{39}Ar$ dates of volcanic rocks that demonstrate latest Miocene–Pliocene remnants of the Miocene drainages (Fig. 2 and Table 2).

GSA Bulletin; https://doi.org/10.1130/B36563.1; 15 figures; 4 tables; 1 supplemental file.

Finally, we discuss how intraplate transtensional faulting and volcanism produced hydrologic barriers, fragmented the fluvial network, and yielded a new system of endorheic basins. Formation of the endorheic basins isolated previously interbreeding springsnail and pupfish populations, leading to the evolution of endemic species in the region's modern springs.

BACKGROUND

Review of Middle to Late Cenozoic Paleogeography

During middle Miocene times (ca. 16–11 Ma), the area now occupied by the southwestern Great Basin was characterized by a generally south- to southeast-directed paleo-fluvial gradient that originated along a drainage divide in the west (Fig. 1 and Table 1). Oligocene to late Miocene erosional surfaces record relatively high-elevation, moderate-relief (525 ± 175 m; Jayko, 2009) topography that was actively eroding, whereas contemporaneous fluviolacustrine basins in the east and southeast (Fig. 1) received sediment predominately from western and northern highlands and locally derived fanglomerates (Table 1; Jayko, 2009; Fridrich and Thompson, 2011).

Lava flows and pumice clasts sourced in the eastern Sierra Nevada region flowed east and west, respectively (see Figs. 1A and 1B), from the area now occupied by the White Mountains and northern Owens Valley, defining a local middle Miocene paleo-divide (e.g., Huber, 1981; Phillips et al., 2011). If this divide also existed from middle Eocene to early Miocene times (e.g., Zhou and Liu, 2019), then it was likely the southern extension of a province-scale, north- to northeast-trending paleo-divide that ran through western and central Nevada and separated the regional Nevadaplano into east- and west-draining fluvial systems (Busby and Putirka, 2009; Henry et al., 2012; Busby et al., 2016).

The existence of middle Eocene to Miocene (ca. 40–12 Ma) fluvio-lacustrine sedimentary rocks east of Death Valley (Figs. 1 and 2; e.g., Reynolds, 1969; Fridrich and Thompson, 2011; Niemi, 2012; Miller et al., 2022) and contemporaneous marine rocks along the southwestern edge of the Sierra Nevada (e.g., Dibblee, 1962; Dibblee and Minch, 2008) that are separated by the relatively high-elevation composite Lindgren-Inyo erosional surface (Fig. 1; Jayko, 2009) supports the presence of the divide before Miocene time.

Miocene sedimentary and volcanic rocks deposited on the Inyo surface and in the eastern fluvio-lacustrine basins record a south- to southeast-directed fluvial course (Fig. 1 and Table 1). Clasts of fluvial conglomerates and sandstones within eastern basins have unique western and northern provenances as well as predominately east- to south-directed paleocurrent indicators (Fig. 1; Table 1). Taken together, the paths shown in Figure 1 and detailed in Table 1 define an apparent interconnected network of fluvio-lacustrine drainages (Figs. 1 and 2).

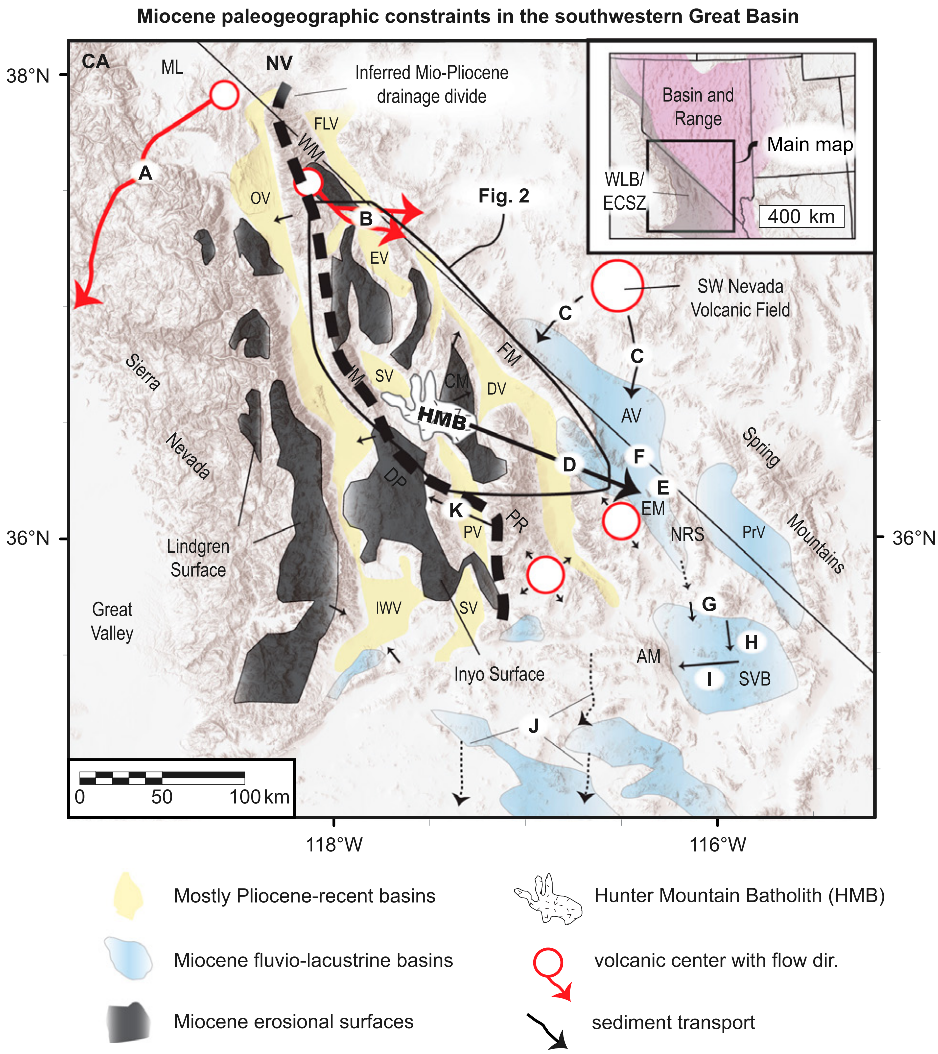

Figure 1. Shaded relief map shows Miocene paleogeographic constraints in the southwestern Great Basin. Letters correspond to descriptions in Table 1. Overall perhaps SE-draining system is consistent with paleo-topographic reconstructions (e.g., Bahadori et al., 2018; Zhou and Liu, 2019). AM—Avawatz Mountains; AV—Amargosa Valley; CM—Cottonwood Mountains; DP—Darwin Plateau; DV—Death Valley; EV—Eureka Valley; EM—Eagle Mountain; FLV—Fish Lake Valley; FM—Funeral Mountains; HMB—Hunter Mountain Batholith; IM—Inyo Mountains; IWV—Indian Wells Valley; ML—Mono Lake; NRS—Nopah-Resting Spring Range; OV—Owens Valley; PR—Panamint Range; PV—Panamint Valley; PrV—Pahrump Valley; SV—Saline Valley; SVB—Shadow Valley Basin; WLB/ECSZ—Walker Lane Belt/Eastern California Shear Zone; WM—White Mountains.

Hunter Mountain Batholith Clasts in Miocene Rocks

The ca. 175 Ma Hunter Mountain Batholith in the southern part of the Cottonwood Mountains (Figs. 1–3) is a distinct lithologic source in the southwestern Great Basin (e.g., Niemi et al., 2001; Dunne and Walker, 2004). The Hunter Mountain Batholith is a multiphase intrusive body with lithology that varies from monzonite to leuco-gabbro and ages spanning ca. 155–180 Ma (see fig. 10 in Niemi et al., 2001).

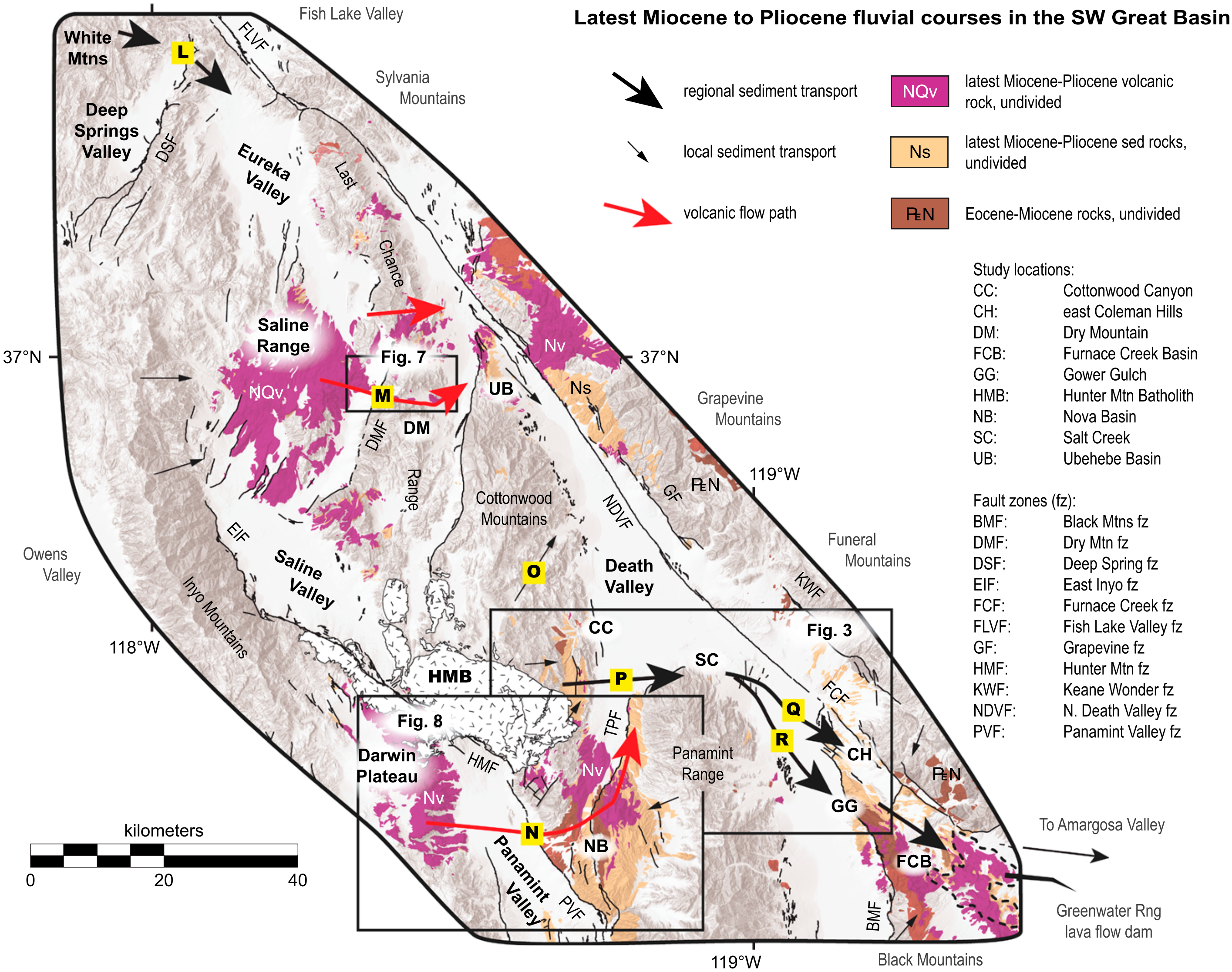

Figure 2. Map shows latest Miocene to Pliocene drainages in the southwestern Great Basin. Letters in yellow boxes correspond to fluvial courses in Table 2. The hatch pattern indicates the ca. 175 Ma Jurassic Hunter Mountain Batholith (HMB). The Greenwater Range lava flow dam is inferred to have disconnected the SE-flowing drainage from the Amargosa Basin (see text in Death Valley Paleogeography section for discussion). TPF—Towne Pass fault zone.

However, ca. 175 Ma is the accepted age of the main quartz monzonite phase of the batholith (Niemi, 2013).

Hunter Mountain Batholith clasts are found within Miocene sedimentary rocks of the Eagle Mountain Formation (Niemi et al., 2001) in southeastern Amargosa Valley (E in Fig. 1 and Table 1) and within the Furnace Creek Basin of Death Valley (Wright et al., 1999). These Hunter Mountain Batholith-bearing deposits preserve a fluvial connection that predates the topographic low of modern Death Valley that now separates the Black Mountains from the Cottonwood Mountains (Figs. 1–3).

The ca. 11.4–13.4 Ma part of the Eagle Mountain Formation (Niemi et al., 2001) contains alluvial fan (Niemi et al., 2001) or distal braided fluvial (Renik et al., 2008) conglomerates with Hunter Mountain Batholith clasts. Conglomerate clasts include >1-m-diameter boulders of Hunter Mountain Batholith (Niemi et al., 2001). Niemi et al. (2001) correlated the boulders to the Hunter Mountain Batholith based on composition and U/Pb zircon dates. Renik et al. (2008) found mostly south- to southeast-directed paleocurrent indicators within the Eagle Mountain Formation conglomerates, which is consistent with the east–southeast fluvial course.

Wright et al. (1999) observed quartz monzonite clasts in the upper part (ca. 12.7–10.6 Ma) of the middle to late Miocene Artist Drive Formation (see D in Fig. 1 and Table 1; Wright et al., 1999). They suspected the clasts were from the Hunter Mountain Batholith. The conglomerates are debris flows with poorly sorted, angular to moderately well rounded, and matrix-supported cobbles to boulders of quartz monzonite and meta-carbonate (Wright et al., 1999). Wright et al. (1999) interpreted the southeast-directed paleocurrent indicators as evidence of northwest–southeast flow from the southern Cottonwood Mountains.

Combined tectonic and sedimentary transport have been proposed to explain the presence of Hunter Mountain Batholith clasts in Miocene rocks east of Death Valley. Presently, the Hunter Mountain Batholith lies ~60–70 km and ~100 km from the Artist Drive and Eagle

TABLE 1. EVIDENCE OF MIOCENE PALEO-DIVIDE AND GENERALLY SOUTHEAST-DIRECTED FLUVIAL COURSES

Path (see Fig. 1)	Formation/name	Age (Ma)	Detail	References
(A) Mono Lake area to San Joaquin River	Undefined	11.4	Andesitic pumice pebbles in sediments underlying the ca. 10 Ma trachyandesite of Kennedy Table; inferred source is east of Mono Lake	Gilbert et al. (1968); Huber (1981)
(B) White Mountains	Tres Plumas basalt	11.5	The Tres Plumas basalts in the White Mountains flowed to the Sylvania Mountains prior to opening Fish Lake Valley	Avila et al. (2018); Mueller (2019)
(C) Amargosa Valley area	Panuga Formation; Horse Spring Formation, and Rocks of Pavits Spring	ca. 16–12.8	Green conglomerate of Panuga Formation; upper member of rocks of Pavits Spring; braided stream deposits; N source recorded by rounded cobbles in conglomerate derived from sources in central SW Nevada	Barnes et al. (1982); Snow and Lux, 1999); Murray et al. (2002); Niemi (2012)
(D) Desolation Canyon and Billie Mine	Artist Drive Formation	12.7–10.6	Lower sedimentary member contains Hunter Mountain Batholith clasts and SE paleocurrent data.	McAllister (1970, 1971); Wright et al. (1999)
(E) Eagle Mountain	Eagle Mountain Formation	13.4–11.6	Te2 member; N and W source recorded by Hunter Mountain Batholith; S- and SE-directed paleocurrent data (some N and E)	Niemi et al. (2001); Renik et al. (2008)
(F) SE Funeral Mountains	Kelly's Well Limestone and Bat Mountain Formation	?? –13.5	Braided stream and fan deposits; sparse N- and NW-directed paleocurrent data; limestone deposited at 1000 ± 500 m paleo-elevation	Cemen et al. (1985); Çemen et al. (1999); Lechler et al. (2013)
(G) Dumont Hills	Dumont Hills and China Ranch Basin	ca. 12–10	Braided stream deposits; S- and SE-directed paleocurrent data	Prave and McMackin (1999)
(H) Shadow Valley	Shadow Valley Basin	ca. 16–11	Mixed fanglomerate and braided stream deposits; W-, SW-, and E-directed paleocurrent data	Fowler (1992); Fowler et al. (1995) Fowler and Calzia (1999); Friedmann (1999)
(I) Avawatz Mountains	Avawatz and Military Canyon formations	ca. 21–12	Lower member; mixed fanglomerate and braided stream deposits; clasts sourced from the Halloran Hills to the E (possibly NE in Miocene time)	Spencer (1990); Brady and Troxel (1999)
(J) Mojave Block	Undefined	11–10	Stream deposits flowed into the Crowder Basin and marginal marine basin to south	Cox et al. (2003)
(K) Argus Range	Undefined	Pre-7.7	Fanglomerates in Argus Range with schist and gneiss clasts most likely derived from the central Panamint Range and granitic clasts derived locally within the Argus Range	Schweig (1989)

Mountain formation outcrops, respectively (D and E in Fig. 1), with the Death Valley, the Black Mountains, and Greenwater Range lying between them. Niemi et al. (2001) and Niemi (2013) suggested that Eagle Mountain was <20 km from the Hunter Mountain Batholith at ca. 11.4 Ma, which indicates ~80–100 km of NW-directed tectonic transport since then (Fig. 1). This is consistent with several tectonic reconstructions, based on independent lines of evidence (Stewart, 1983; Wernicke et al., 1988; Snow and Wernicke, 2000; Andrew, 2010; Lutz et al., 2021; Lutz et al., 2022). However, the presence of quartz-monzonite clasts and southeast-directed paleocurrent indicators in ca. 12.7–10.6 Ma rocks at the Desolation Canyon and Billie Mine localities (D in Fig. 1) suggests a maximum of 60–70 km of tectonic transport of the Hunter Mountain Batholith, and 30–40 km of sedimentary transport between the Artist Drive and Eagle Mountain formations.

Latest Miocene to Pliocene Conglomerates of the Furnace Creek Formation

Conglomerates of the Furnace Creek Formation preserve the latest Miocene to Pliocene (ca. 6.5–3.5 Ma) evolution of fluvial drainages in Death Valley (McAllister, 1970; Wright and Troxel, 1993; Wright et al., 1999; Fridrich et al., 2012). Furnace Creek Formation conglomerates are well-exposed at Gower Gulch (Figs. 3 and 4), the East Coleman Hills (Figs. 3 and 5), and Salt Creek (Figs. 3 and 6). The Gower Gulch and the East Coleman Hills sites are located in the northern Black Mountains, and the Salt Creek site is at the northeastern end of the Panamint Range (Fig. 3).

Gower Gulch

The Conglomerate of Gower Gulch (Wright et al., 1999; Nfc in Fig. 4), like underlying fluvial arkosic sandstones and debris flows within the Artist Drive Formation, records fluvial connection between the Cottonwood Mountains and Furnace Creek Basin during deposition (see path P to R in Fig. 2 and Table 2). The conglomerate contains Hunter Mountain Batholith-like quartz monzonite clasts and rare southeast-directed paleocurrent indicators (Wright et al., 1999; Fridrich et al., 2012). Wright et al. (1999) described the Conglomerate of Gower Gulch as torrent-related debrites, based on very poor sorting, crude layering, and matrix support of pebble- to small boulder-sized clasts. Fridrich et al. (2012) reported well-rounded to subrounded clasts of similar size and composition. Clasts

TABLE 2. EVIDENCE OF MIO-PLIOCENE FLUVIAL CONNECTIONS IN THE SW GREAT BASIN

Path (see Fig. 2)	Age (Ma)	Detail	References
(L) White-Inyo Range	pre-3.1 (?)	Fluvial conglomerates in White Mountains record flow toward Eureka Valley; predate Deep Springs Valley; lack of White Mountains' detritus in Fish Lake Valley basin prior to ca. 3 Ma	Reheis and Sawyer (1997); Mueller (2019); Knott et al. (2019)
(M) Saline Range/Dry Mountain	pre-3.9	Nb basalt flowed east through valley from Saline Range to Death Valley at ca. 3.92 Ma; existing low recorded by ca. 4.51 Ma andesite cone and regional SE-directed Miocene fluvial system (see Fig. 1)	This study; Burchfiel (1969); Sternlof (1988)
(N) Nova Basin	pre-3.9	Basaltic trachy-andesite of Black Point flowed from Darwin Plateau to Death Valley	This study; Coleman and Walker (1990)
(O) N Cottonwood Mountains	ca. 6.2–3.7	Sandy, clast-supported conglomerates in Marble Canyon with Pennsylvanian–Permian clasts from the S Cottonwood Mountains	Snow and Lux (1999)
(P) W of Salt Creek	ca. 6.9–4.9	HMB† clasts in conglomerate west of Salt Creek	This study; Wright and Troxel (1993)
(Q) E Coleman Hills	ca. 4.2–3.5	Hunter Mountain Batholith clasts in upper Furnace Creek Formation Conglomerate	This study
(R) Gower Gulch	ca. 8.1–6.2	HMB† clasts in Conglomerate of Gower Gulch	This study; Wright et al. (1999)

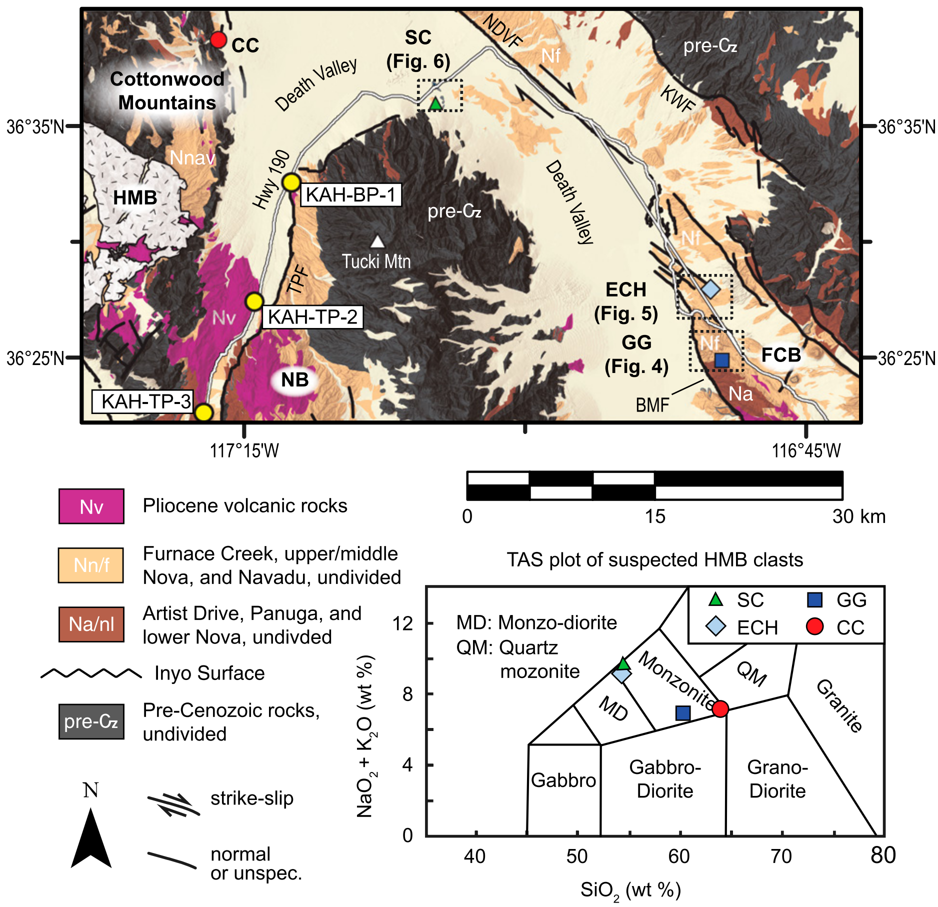

Figure 3. Geologic map of the north-central Death Valley area shows the Hunter Mountain Batholith (HMB; hatch pattern), study locations where probable Hunter Mountain Batholith clasts are present in conglomerates of the Furnace Creek Formation (dashed boxes), and sample locations where probable Hunter Mountain Batholith clasts were analyzed (see TAS plot). Yellow circles are sample locations of lava flows within the Nova Basin (see Fig. 8 for details). CC—Cottonwood Canyon; ECH—East Coleman Hills; FCB—Furnace Creek Basin; GG—Gower Gulch; NB—Nova Basin; SC—Salt Creek; Nnav—Navadu Formation. Geology after Workman et al. (2016). BMF—Black Mountains fault; NDVF—Northern Death Valley fault; KWF—Keane Wonder fault; TPF—Towne Pass fault.

are predominately Paleozoic carbonate and chert, with minor reworked Miocene volcanic and sedimentary rocks of the underlying Artist Drive Formation, and quartz monzonite (Fig. 4) (Wright et al., 1999; Fridrich et al., 2012).

The age of the Conglomerate of Gower Gulch is poorly constrained. McAllister (1970) mapped the conglomerate as the base of the Furnace Creek Formation (Nfc in Fig. 4), whereas Wright et al. (1999) assigned this same conglomerate to the upper Artist Drive Formation (Na in Fig. 4). The conglomerate is well-exposed at the western front of the Black Mountains and underlies several basalt flows, one of which was dated at 5.87 ± 0.12 Ma (Muessig et al., 2019).

East Coleman Hills

Conglomerates within the upper part of the Furnace Creek Formation are well-exposed in the East Coleman Hills within the Texas Spring Syncline (Fig. 5). McAllister (1970) mapped Tfcu (Nfcu in Fig. 5) in the northeast limb of the syncline in the colemanite-bearing portion of the Furnace Creek Formation. Based on McAllister's (1970) mapping and Knott et al.'s (2005; 2018) tephrochronology, the Nfcu unit is stratigraphically below the ca. 3.54–3.21 Ma uppermost part of the Furnace Creek Formation (Nfu and Nft). Knott et al. (2018) showed that the top of the main body member of the Furnace Creek Formation (Nf in Fig. 5; Tf of Fridrich et al., 2012), which underlies the Nfcu unit, is 4.187 Ma. These data suggest that unit Nfcu is ca. 4.19–3.54 Ma.

Salt Creek

Wright and Troxel (1993) mapped conglomerate beds within the Furnace Creek Formation west of Salt Creek (their QTfc) and noted the prominence of Hunter Mountain Batholith clasts. A Quaternary or Pliocene lava flow (their QTb; Nfand in Fig. 6) overlies the conglomerate. The lava flow was dated at 4.8 ± 0.8 Ma (whole-rock K-Ar; L.A. Wright, 1998, personal commun.).

Volcanic Rocks in the Dry Mountain Area and Nova Basin

Dry Mountain

In an east- to west-trending valley across the southern Last Chance Range, ~5 km north of Dry Mountain, Burchfiel (1969) mapped a Plio-Pleistocene basalt flow filling the valley (Nb and dark green in Fig. 7). Burchfiel (1969) noted flow structures within the "basalt tongue" that showed a west–east flow direction. He inferred that the basalt erupted in the Saline Range, and that Dry Mountain was uplifted relative to Saline Valley after eruption. Several Neogene basalt outcrops are mapped in the eastern Saline Range, across the alluvial piedmont west of the valley, but Burchfiel (1969) did not correlate any of these basalt outcrops to the "basalt tongue." Sternlof (1988) dated the basalt tongue at 3.17 ± 0.12 Ma (whole-rock, K-Ar). At the eastern end of the valley, Burchfiel (1969) mapped a 3 km^2 Neogene basalt cone with related flows (Nv or "andesite cone" in Fig. 7).

About 12 km north of Dry Mountain, Wrucke and Corbett (1990) mapped Neogene (Tertiary) volcanic rocks that erupted in the Saline Range, flowed east across what is presently the Last Chance Range, onto the eastern piedmont, and into Death Valley (red arrow north of path M in Fig. 2). These are olivine basalt to trachybasalt dated at ca. 4.2 ± 0.3 Ma to 4.6 ± 0.3 Ma (whole rock K-Ar; Elliott et al., 1984).

Nova Basin

The Neogene Nova Formation was deposited in the Nova Basin between the northern Panamint Range and southern Cottonwood Mountains (Hunt and Mabey, 1966; Hall, 1971; Hodges et al., 1989). The Nova Formation (Nnl, m, and u in Fig. 8) consists of conglomerate, sandstone, and megabreccia with intercalated volcanic flows (Hodges et al., 1989). The megabreccia and conglomerates record erosion of the Panamint Mountains to the southeast (Hall, 1971; Hodges et al., 1989; Fig. 3). Neither Hall (1971) nor Hodges et al. (1989) mentioned the presence of clasts from the Hunter Mountain Batholith, which

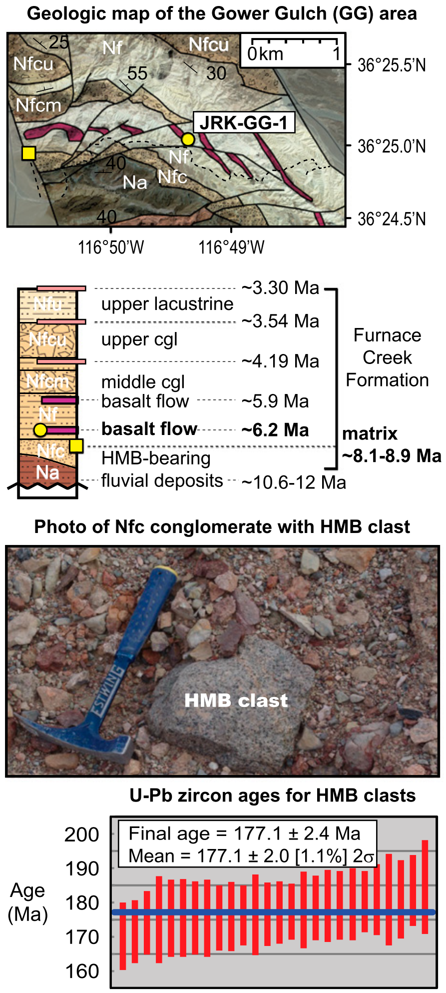

Figure 4. Details of the Gower Gulch area are shown. Nfc/m/u—lower/middle/upper conglomerate of the Furnace Creek Formation; Na—Artist Drive Formation; cgl—conglomerate. Yellow circles and squares are lava flow and conglomerate matrix sample locations, respectively. Bold text in the stratigraphic column indicates new dates reported in this study. Other ages and general stratigraphy are after Knott et al. (2018), Wright et al. (1999), and Muessig et al. (2019). Mapping is after Fridrich et al. (2012) and McAllister (1970). HMB—Hunter Mountain Batholith.

is exposed 15 km to the north–northwest (Figs. 2, 3, and 8), within the Nova Formation conglomerates. Geochemical data indicate that the volcanic flows erupted from the Darwin Plateau volcanic field in the Argus Range west of Panamint Valley (path N in Fig. 2; Coleman and Walker, 1990).

Lava flows in the Nova Basin were dated previously at ca. 3.5–5.8 Ma by K-Ar dating (Hall, 1971; Larson, 1979; Hodges et al., 1989) and re-dated at ca. 3.5–7.2 Ma by $^{40}Ar/^{39}Ar$ dating (Snyder and Hodges, 2000; Fig. 8 and Table 3). Some of the $^{40}Ar/^{39}Ar$ ages, however, were based on imprecise age spectra (e.g., samples NB-2, NB-3, and NB-4) and/or isochron ages that incorporated heating steps with large errors (e.g., NB-5).

METHODS

Traditional field methods of mapping, observation, and sampling were applied to the specific study areas (see Fig. 2). Samples of volcanic groundmass, granitoid clasts, and/or conglomerate matrix were collected for geochronology and major/trace-element geochemistry.

Zircon U/Pb Dating

Clasts and sandy matrix of conglomerates at Salt Creek, East Coleman Hills, and Gower Gulch were dated using zircon U/Pb methods, following the procedures described in Gehrels (2014) and references therein (see Supplemental Material[1]). Detrital zircons were separated at California State University, Fullerton, California, USA, using standard mineral separation techniques, which leverage the characteristic high density and low magnetism of zircon. Zircon mounts were prepared and imaged by cathodoluminescence at the Arizona LaserChron Center, Tucson, Arizona, USA; zircon U-Pb geochronology was conducted using high-resolution laser ablation–inductively coupled plasma–mass spectrometry on a Thermo Scientific Element 2 instrument (Gehrels et al., 2006, 2008). U-Pb isotopic data were reduced with 20% discordance and 5% reverse discordance filters using E2agecalc. Approximately 20–30 and 250 zircons were analyzed from clast and matrix samples, respectively.

X-Ray Fluorescence

Volcanic samples and granitoid clasts from the Furnace Creek Formation were collected for whole-rock X-ray fluorescence (XRF) analysis to determine their major, minor, and trace-element compositions. Samples were crushed and powdered at California State University, Fullerton. At Pomona College, Claremont, California, di-lithium tetraborate flux was added to the powders, which were fused twice in graphite crucibles, to maximize homogeneity of the glass beads, which then were analyzed on a Panalytical Axios X-ray fluorescence spectrometer.

[1]Supplemental Material. Text: Argon analytical methods. Table S1: Trace element concentrations of igneous rocks and igneous rock clasts in Death Valley region. Figure S1: Total Alkali-Silica plot of volcanic rocks sampled in this study. Figure S2: Spider diagram plot of volcanic rocks sampled in this study. Data 1: Zircon U-Pb data. Data 2: Analytical Settings for U-Pb Geochronology at the Arizona LaserChron Center (Element 2 Single Collector). Data 3: Sanidine ^{40}Ar-^{39}Ar data Data 4: Groundmass ^{40}Ar-^{39}Ar data. Please visit https://doi.org/10.1130/GSAB.S.21266346 to access the supplemental material, and contact editing@geosociety.org with any questions.

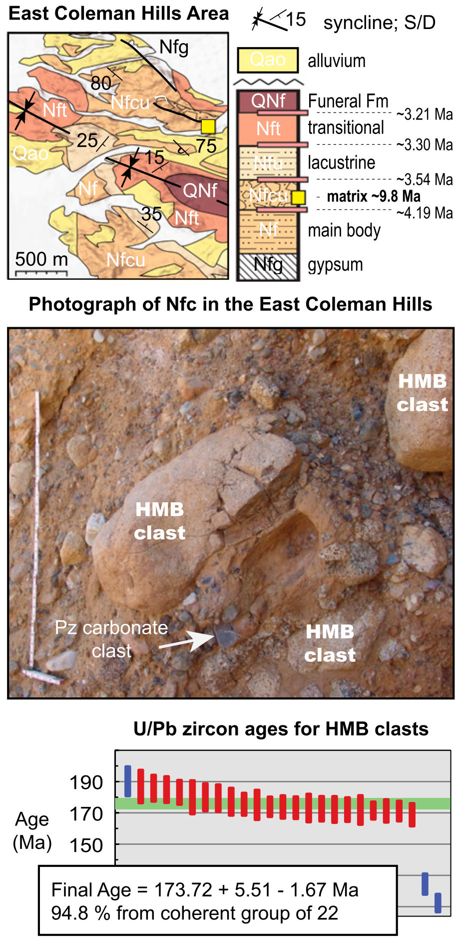

Figure 5. Diagrams show details of the East Coleman Hills area. Mapping and stratigraphy are after McAllister (1970) and Knott et al. (2018), respectively. HMB—Hunter Mountain Batholith; Nfc/m/u—lower/middle/upper conglomerate of the Furnace Creek Formation; Qao—Quaternary alluvium; QNf—Neogene–Quaternary Funeral Formation; Nft—transitional member of Furnace Creek Formation; Nfg—gypsum member of Furnace Creek Formation.

$^{40}Ar/^{39}Ar$ Dating

Samples of volcanic rocks and conglomerate matrix from the Furnace Creek Formation

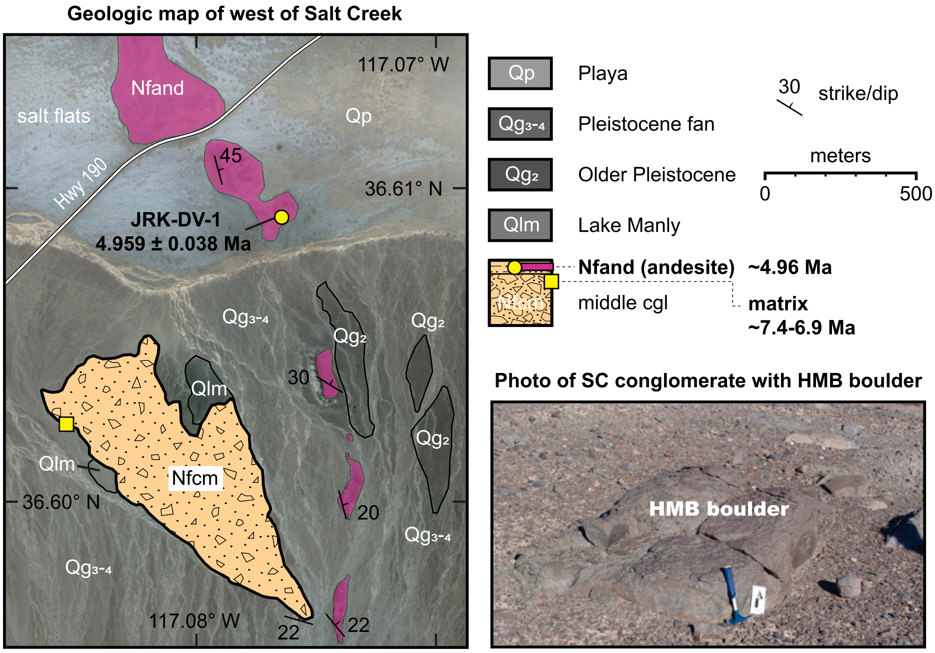

Figure 6. Details of the area west of Salt Creek (SC) are shown. Mapping is by J.R. Knott. Yellow circles and squares are lava flow and conglomerate matrix sample locations, respectively. Nfcm—middle conglomerate (?) of the Furnace Creek Formation; HMB—Hunter Mountain Batholith; cgl—conglomerate.

were collected for $^{40}Ar/^{39}Ar$ dating at the New Mexico Geochronology Research Laboratory (NMGRL), Socorro, New Mexico, USA. We dated volcanic groundmass and detrital-matrix K-feldspar grains.

Volcanic groundmass was prepared for irradiation using standard mineral separation methods. Samples were crushed and sieved. Magnetic grains were separated. Two aliquots of groundmass per sample (~40 g) were hand-picked to eliminate phenocrystic contamination. Groundmass samples were loaded into machined aluminum discs and irradiated in a TRIGA Reactor at either Denver, Colorado, USA (USGS) or Oregon State University, Corvallis, Oregon, USA (see Supplemental Material for a full description of irradiation times and geometries for each sample; see footnote 1).

Eruption ages of intermediate to mafic volcanic rocks were estimated by incremental step-heating experiments performed on the Felix system at NMGRL (see Supplemental Material for more details). Groundmass samples were heated in typical 45 s steps, followed by 60 s of gas clean up with an SAES GP-50 getter operated at 2 A. Isotopes of argon were measured using a Thermo Scientific HELIX MC Plus multicollector–mass spectrometer. Isotopes ^{40}Ar, ^{39}Ar, ^{38}Ar, and ^{37}Ar were measured on Faraday collectors, whereas ^{36}Ar was measured on a compact discrete dynode (CDD) ion counter.

Detrital K-feldspar crystals and neutron flux monitors were dated by single crystal laser fusion (SCLF) utilizing the Jan system at NMGRL (see Supplemental Material for more details). Crystals were fused with a CO_2 laser. Extracted gas was cleaned with a variety of getter configurations. Cleaned gas was then analyzed using a Thermo Scientific Argus VI multicollector-mass spectrometer.

Isotopes of low-concentration samples were collected for 280–400 s followed by 45 s of baseline measurement. High-concentration samples (large unknown grains and FC-2) were measured using 120 s of isotope collection followed by 30–60 s of baseline measurement. Analyses were truncated based on various criteria to facilitate efficient data collection. For instance, relatively old grains that did not contribute significantly to maximum depositional age determination or provenance were analyzed for durations of typically less than 60 s. Basalt samples used 340 s of data collection followed by 60 s of baseline measurement.

Data were collected and reduced with in-house Pychron software and MassSpec version 7.875, respectively (see Supplemental Material for all data tables). Fish Canyon Tuff sanidine (FC-2) with an assigned age of 28.201 Ma (Kuiper et al., 2008) was used as a neutron flux monitor. A ^{40}K decay constant of 5.463e-10/a was used (Min et al., 2000) with isotope abundances after Steiger and Jäger (1977).

RESULTS

Hunter Mountain Batholith Clasts in the Furnace Creek Formation and at Cottonwood Canyon

We found granitoid boulders in the Furnace Creek Formation at Gower Gulch, East Coleman Hills, and Salt Creek (Figs. 3–6). Total alkali versus silica plots from XRF analyses show that all granitoid clasts, including those eroding directly from the Hunter Mountain Batholith at Cottonwood Canyon (Figs. 2 and 3), are monzonite (Fig. 3). The U/Pb zircon ages of monzonite clasts from Furnace Creek Formation Conglomerate at Gower Gulch and Coleman Hills are 177.1 ± 2.4 Ma (Fig. 4) and 173.72 (+5.51 –1.67) Ma (Fig. 5), respectively. These ca. 172–179 Ma dates and monzonite rock types are within error of the Hunter Mountain Batholith (Niemi et al., 2001; Niemi, 2013), which strongly supports that the monzonite clasts in the Furnace Creek Formation conglomerates are from the Hunter Mountain Batholith.

Deposition and provenance of the Furnace Creek Formation

Conglomerate of Gower Gulch or Lower Furnace Creek Formation

Lithology and deposition. The Conglomerate at Gower Gulch includes subrounded to rounded, gravel- to cobble-sized clasts of Paleozoic carbonate, volcanic rock, and Hunter Mountain Batholith in a sand matrix (Fig. 4). The conglomerate is mostly clast supported and poorly bedded. Granitoid rocks make up ~10% of the clasts, consistent with the data presented by Wright et al. (1999). Our outcrop observations confirm Wright et al.'s (1999) interpretation that these are debris-flow deposits in a braided stream setting. Microscopically, we found rounded to subrounded sanidine crystals in the Conglomerate of Gower Gulch matrix, which supports the fluvial interpretation.

Stratigraphic age. We determined a whole-rock $^{40}Ar/^{39}Ar$ date of 6.197 ± 0.020 Ma for the basalt (Tfb of McAllister, 1970, and Fridrich et al., 2012) intercalated with Furnace Creek Formation sediments overlying the Conglomerate of Gower Gulch (Fig. 9B and Table 3).

Detrital zircon and feldspar. The distribution of detrital K-feldspar and zircon ages from the Conglomerate of Gower Gulch is broad (Fig. 10; also see Supplemental Material), which suggests a mixed-provenance fluvial system. Detrital zircons in the Conglomerate of Gower Gulch matrix ranged in age from 2.9 Ga to 7.1 ± 0.2 Ma. Of the 254 zircons analyzed, 21 crystals (8%) had dates that exceeded 1 Ga.

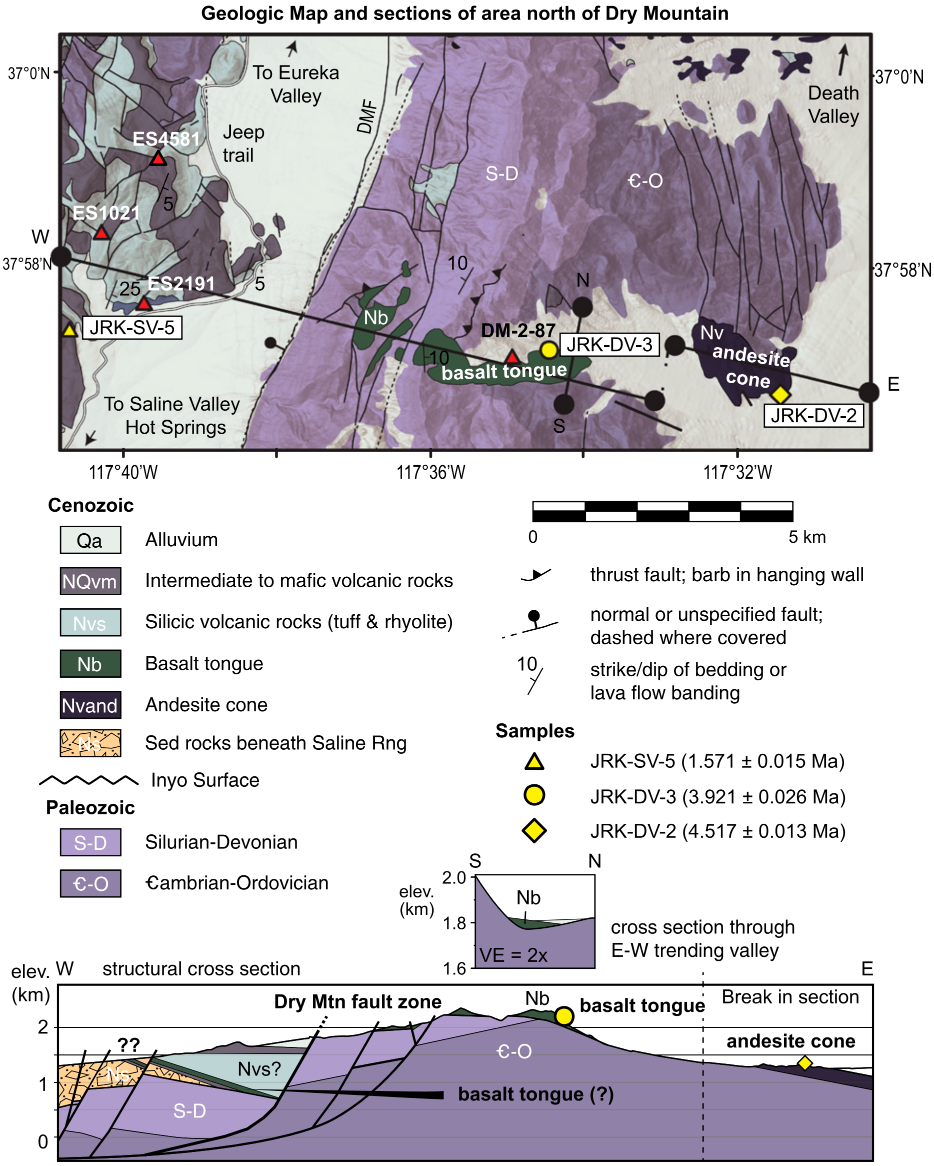

Figure 7. Geologic map and sections of the area north of Dry Mountain in the southern Last Chance Range show key lava flows that constrain the age of the east–west valley that connected the Saline Range and Death Valley. Yellow symbols are samples from this study. Red triangles are previous sample locations from Elliott et al. (1984) and Sternlof (1988). Dates are reported in Table 3. Depth to bedrock in the structural cross section (bottom) is after Blakely et al. (1999). DMF—Dry Mountain fault zone. Mapping is after Workman et al. (2016) and Burchfiel (1969).

There is a dominant peak in the zircon probability distribution at ca. 175 Ma (Fig. 10B), which is the accepted age for the main monzonitic phase of the Hunter Mountain Batholith (e.g., Niemi, 2013). Approximately 22% (55/253) of the detrital zircons fall within error of 155–180 Ma (Fig. 10B; also see Supplemental Material). These could be from Hunter Mountain Batholith or other Jurassic intrusive rocks exposed farther west in the White, Inyo, Argus, and Slate Ranges (Fig. 11). The youngest grain dated was 8.1 ± 0.3 Ma and is considered the maximum depositional age.

Eighty-one detrital K-feldspar grains from the Conglomerate of Gower Gulch matrix were dated by the $^{40}Ar/^{39}Ar$ method. Dates ranged from 158 Ma to 8.99 Ma. There is a major peak at ca. 11.4 Ma, which most likely represents eruptions from the southwest Nevada volcanic field. The youngest acceptable grain date was 8.990 ± 0.046 Ma.

East Coleman Hills Conglomerate

Lithology and deposition. The conglomerate in the East Coleman Hills is massive, poorly sorted, poorly bedded, and matrix-supported, which is consistent with deposition as a debris flow (Fig. 5). Subrounded to angular monzonite clasts range in size from gravels to boulders (up to 1 m diameter). The contact between the conglomerate and surrounding, finer-grained member of the Furnace Creek Formation (unit Nf; Fig. 5) is abrupt where exposed, and disconformable.

Stratigraphic Age. Faulting and folding complicate stratigraphic age determination. Our field observations did not improve the ca. 4.19–3.54 Ma stratigraphic age of the upper conglomerate member of the Furnace Creek Formation (Nfcu) unit based on previous mapping by McAllister (1970) and constraints in Knott et al. (2018).

Detrital zircon and feldspar. The detrital K-feldspar and zircon grains from the conglomerate in the East Coleman Hills inform the provenance assessment. Detrital zircon U/Pb ages range from 2.6 Ga to ca. 9.8 Ma with ~68% (167/245) within error of 180–155 Ma (Fig. 10B; see also Supplemental Material). There is a major peak at ca. 175 Ma, with minor peaks at 150–155 Ma, 100 Ma, 85 Ma, and ca. 72 Ma (Fig. 10B). The youngest zircon grain was 9.8 ± 0.1 Ma (Table 4).

The 130 detrital K-feldspar grains analyzed for $^{40}Ar/^{39}Ar$ yielded dates ranging from 199 Ma to 9.76 ± 0.02 Ma (see Supplemental Material). Thirty-seven (28%) K-feldspars yielded dates within error of 180–155 Ma or within the age of the Hunter Mountain Batholith (see Supplemental Material).

Salt Creek

Lithology and deposition. The conglomerate in the Furnace Creek Formation of Wright and Troxel (1993), west of Salt Creek, is massive to poorly bedded and matrix-supported, which is consistent with debris-flow deposition. Clasts are subrounded to angular with many >1.5 m in diameter (Fig. 6B); boulder-sized clasts are exclusively Hunter Mountain Batholith monzonite. XRF data show that the reddish-black volcanic rock overlying the conglomerate is andesite (Nfand in Fig. 6). The flow-banding in the andesite is conformable with the northeast dips of the underlying conglomerate (Fig. 6).

Stratigraphic Age. The minimum age of the conglomerate was determined by the overlying andesite. The whole rock $^{40}Ar/^{39}Ar$ date on the andesite is 4.959 ± 0.038 Ma (Fig. 9A and Table 3).

Detrital zircon and feldspar. Most detrital zircon and K-feldspar dates from the Furnace

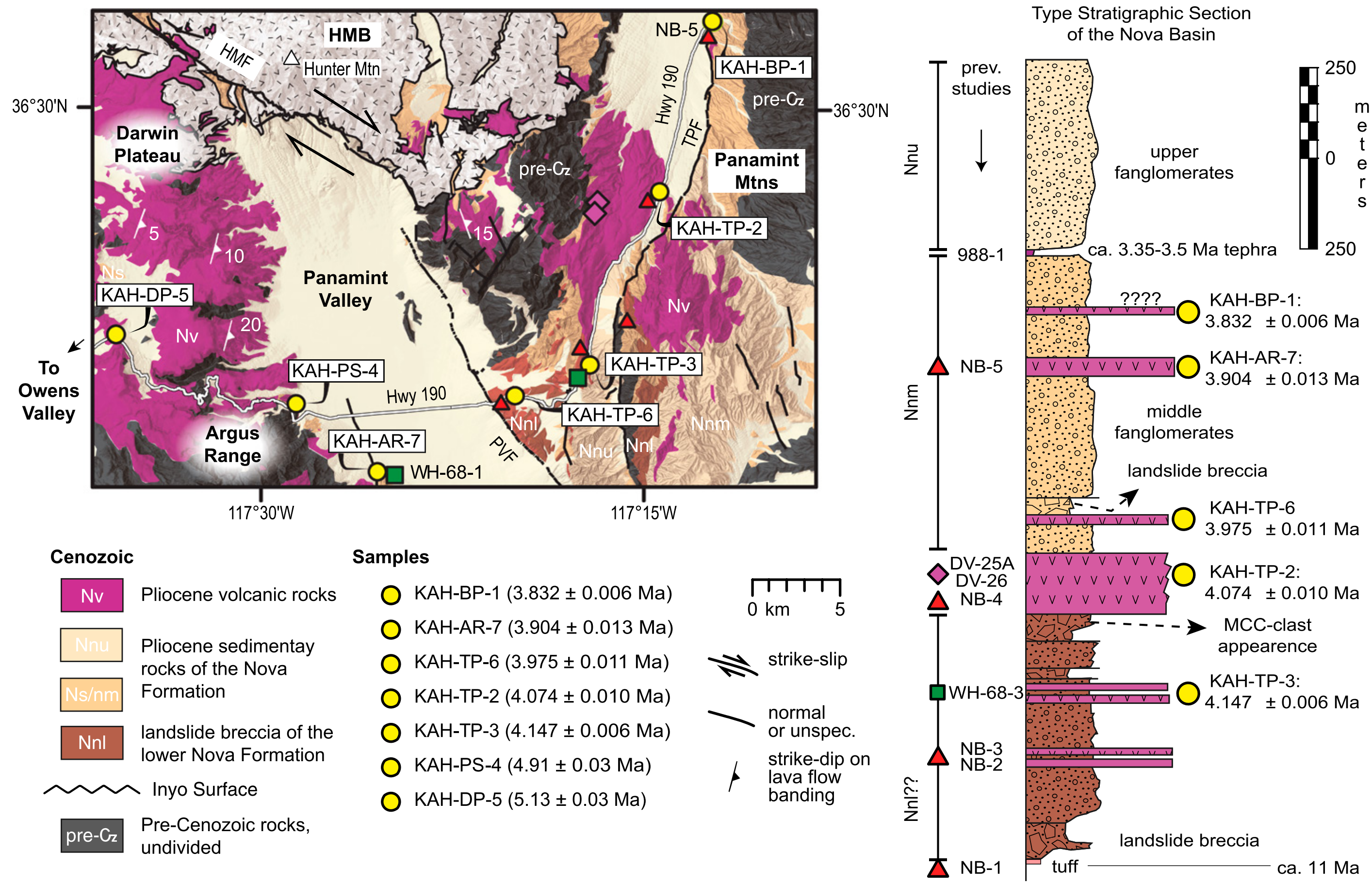

Figure 8. Left: Geologic map of the northern Panamint Valley–Towne Pass area shows lava flows (pink) of the Darwin Plateau and within the Nova Basin. Yellow circles are sample locations from this study. Sample locations from previous studies are shown by green squares (Hall, 1971), red triangles (Snyder and Hodges, 2000), and pink diamonds (Larson, 1979). Ages for those samples are reported in Table 3. The Hunter Mountain Batholith (HMB) is shown by the hatch pattern. HMF—Hunter Mountain fault zone; TPF—Towne Pass fault zone; PVF—Panamint Valley fault zone; MCC—Metamorphic core complex. Right: stratigraphic section of the Nova Basin (after Hodges et al., 1989; Snyder and Hodges, 2000) shows the positions and ages of lava flows.

Creek Formation Conglomerate west of Salt Creek have a relatively narrow range (Fig. 10; also see Supplemental Material). Three hundred and thirteen U/Pb dates were measured on zircons from the conglomerate matrix with dates ranging from 2.5 Ga to ca. 6.9 Ma. Ninety percent (228/2533) of the zircons dated were within error of 180–155 Ma. There is a major peak at ca. 175 Ma, with minor peaks at 150–155 Ma, 100 Ma, 85 Ma, and ca. 72 Ma (Fig. 10B). The spectrum is quite similar to that of the East Coleman Hills, which suggests common provenance. Only nine zircons (3%) were younger than 12.1 Ma. The youngest zircon grain dated was 6.9 ± 0.1 Ma.

The 120 detrital K-feldspar grains analyzed for $^{40}Ar/^{39}Ar$ yielded dates between ca. 205 Ma to ca. 7.5 Ma. There is a major peak at ca. 175 Ma. The youngest acceptable grain dated was 7.47 ± 0.10 Ma.

Dry Mountain, Darwin Plateau, and Nova Basin Volcanic Rocks

Preferred eruption ages of volcanic rocks collected north of Dry Mountain, at the Darwin Plateau and Nova Basin, are presented in Figures 7, 8, 12, and 13 and Table 3. In many cases, age-spectra and inverse isochron analysis indicate that the dated aliquots contained excess argon and a trapped component of atmospheric argon. Detailed explanations of eruption age interpretations, complete data tables, age-spectra, and isochron diagrams are in the Supplemental Material.

Dry Mountain

In the Last Chance Range, north of Dry Mountain, the volcanic cone at the mouth of the east-west–trending canyon is an andesite (Fig. S1 and Table 4) with an $^{40}Ar/^{39}Ar$ date of 4.615 ± 0.013 Ma (Fig. 12 and Table 3). Additional flows that were emitted from the cone and accumulated in the canyon thalweg are black, vesicular basalt. A separate, blocky-to-vesicular basalt flow lies up-gradient and to the west. This flow is 3.921 ± 0.026 Ma (Fig. 12 and Table 3). This western basalt flow is the same flow from which Sternlof (1988) obtained a whole rock, K-Ar date of 3.17 ± 0.12 Ma. Based on the lack of a volcanic center and the geomorphic position, we concur with Burchfiel's (1969) conclusion that the 3.92 Ma basalt flow erupted from the Saline Range.

Nova Basin

Seven $^{40}Ar/^{39}Ar$ dates were determined on basalt to trachyandesite flows (see Table 4 for geochemical data and Fig. S1 for the total alkali silica [TAS] plot) along an east–west transect through the Nova Basin (Fig. 8). The ages of these

TABLE 3. SUMMARY OF MAXIMUM DEPOSITIONAL AGES AND ERUPTION AGES

Sample Name/location	Location Latitude (°N)	Longitude (°W)	Date (Ma)	Type	Previous dates (Ma)
Gower Gulch area					
JRK-GG-1	36.41684	116.82155	6.197 ± 0.020	plateau*	5.87 ± 1.5[#]
Matrix K-spar	36.41376	116.84301	9.022 ± 0.010	SCLF[†]	N.A.
Matrix zircon	36.41376	116.84301	8.1 ± 0.300	LA-ICP-MS[§]	N.A.
East Coleman Hills					
Mesquite Sp. Tuff	N.D.	N.D.	N.D.	N.D.	ca. 3.32**
Matrix K-spar	36.46808	116.83998	9.769 ± 0.019	SCLF[†]	N.A.
Matrix zircon	36.46808	116.83998	9.8 ± 0.100	LA-ICP-MS[§]	N.A.
West of Salt Creek					
JRK-DV-1	36.61059	117.07661	4.959 ± 0.038	plateau	4.8 ± 0.8[††]
Matrix K-spar	36.60292	117.08464	7.438 ± 0.021	SCLF[†]	N.A.
Matrix zircon	36.60292	117.08464	6.9 ± 0.100	LA-ICP-MS[§]	N.A.
Dry Mountain area					
JRK-SV-5	36.96953	117.63334	1.571 ± 0.015	plateau	1.35 ± 0.02[§§]
JRK-DV-3	36.95202	117.57504	3.921 ± 0.026	plateau	3.17 ± 0.12[§§]
JRK-DV-2	36.94520	117.52329	4.517 ± 0.013	plateau*	N.A.
Nova Basin and Darwin Plateau					
KAH-BP-1	36.54647	117.20559	3.832 ± 0.006	plateau	ca. 3.9[##]
KAH-AR-7	36.30798	117.42371	3.904 ± 0.013	plateau*	ca. 4***
KAH-TP-6	36.34832	117.33432	3.975 ± 0.011	isochron	ca. 7.3[##]
KAH-TP-2	36.45629	117.23985	4.074 ± 0.010	plateau*	4.4[##]; 4.3–4.4[†††]
KAH-TP-3	36.36484	117.28542	4.147 ± 0.006	isochron	5.14***; 7.8[##]
KAH-PS-4	36.34373	117.47705	4.91 ± 0.030	isochron	5.2[##]
KAH-DP-5	36.37976	117.59550	5.129 ± 0.026	plateau	N.A.

*Plateau and isochron ages within uncertainty of each other.
[†]SCLF—Single crystal laser fusion.
[§]LA-ICP-MS—Laser ablation–inductively coupled plasma–mass spectrometry.
[#]Cemen et al. (1985).
**Knott et al. (2018).
[††]Calzia, J. (2017, written communication).
[§§]Sternlof (1988).
[##]Snyder and Hodges (2000).
***Hall (1971).
[†††]Larson (1979).
N.D.—not determined.

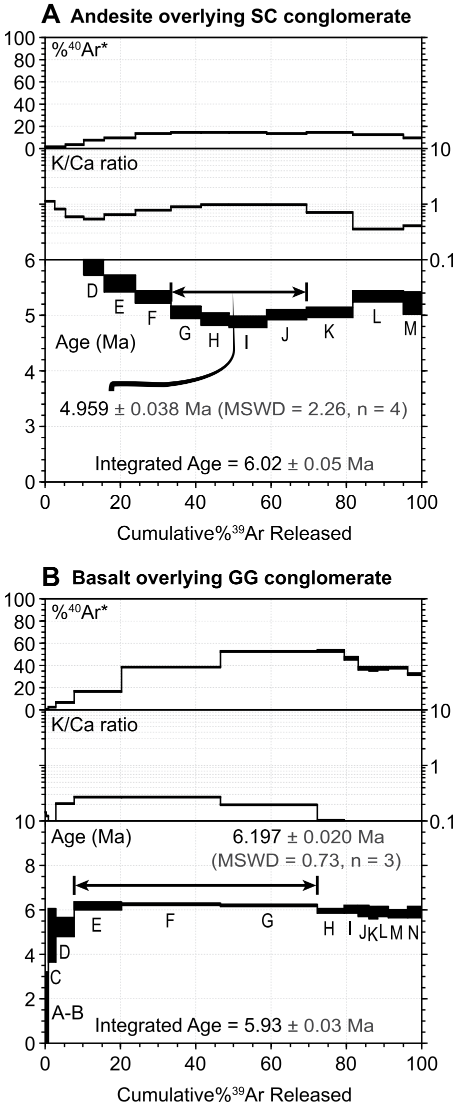

Figure 9. Graphs show age spectra from step-heating experiments performed on groundmass of lava flows overlying the Hunter Mountain Batholith-bearing conglomerates at (A) Salt Creek (SC) and (B) Gower Gulch (GG). MSWD—mean square of weighted deviates.

volcanic rocks ranged from 5.13 ± 0.03 Ma to 3.832 ± 0.006 Ma (Fig. 8 and Table 3). Coleman and Walker (1990) determined geochemically that Nova Basin volcanic rocks erupted from the Darwin Plateau (Fig. 8) and that, most critically, the youngest date of 3.832 ± 0.006 Ma at Black Point (Fig. 13) is in the stratigraphically highest position and farthest east.

Death Valley Paleogeography

Our results support the existence of an interconnected, southeast-draining fluvial system in latest Miocene to Pliocene times. We suggest that the system had headwaters in the White-Inyo Range and extended to the Furnace Creek Basin and Amargosa Valley. The system can be broken up into two distinct fluvial courses (Figs. 14 and 15), with each supported by independent provenance, paleocurrent indicators, and age.

The Northern Fluvial Course

New dates on volcanic rocks in the Dry Mountain area, when combined with previous studies, define a Pliocene (ca. 4.5–3.9 Ma) and topographically viable fluvial course that may have connected the modern White-Inyo Range, Saline Range area, and Death Valley (Figs. 11, 14, and 15). This fluvial course may have existed in Miocene time as well (see Fig. 1 and Table 1), but direct evidence is lacking.

The 3.921 ± 0.026 Ma basalt tongue flowed east from the Saline Range through the trending valley north of Dry Mountain (dark green in Figs. 7 and 12). The valley was a local topographic low by at least 4.517 ± 0.013 Ma, when lava from the andesite cone erupted along the northern flank of the valley and flowed south (andesite in Figs. 7 and 12). These data show that the valley was at a lower elevation than the Saline Range to the west from before ca. 4.5 Ma until ca. 3.9 Ma (Figs. 14 and 15).

We infer that the valley north of Dry Mountain extended west into the area now occupied by the modern Saline Range, Saline Valley, and Eureka Valley (Figs. 14 and 15A), although this inference depends upon how a low gravity anomaly beneath the Saline Range is interpreted. The low gravity anomaly beneath the ca. 4.6–1.45 Ma volcanic rocks in the Saline Range (Elliott et al., 1984; Sternlof, 1988; this study) has been interpreted as either (1) an alluvium-filled basin (Figs. 7 and 14), or (2) low-gravity plutons (Blakely and McKee, 1985; Blakely et al., 1999).

If the gravity low beneath the Saline Range represents a non-terminal Miocene basin, a topographic low extended from the eastern edge of the modern White-Inyo Range to the valley north of modern-day Dry Mountain at ca. 4.6 Ma (see paths labeled M in Figs. 2, 14, and 15A). Alternatively, if the gravity low beneath the Saline Range represents a Miocene terminal basin, east-directed flow of lava through the valley north of Dry Mountain (Fig. 7) could indicate that the basin was filled and overtopped.

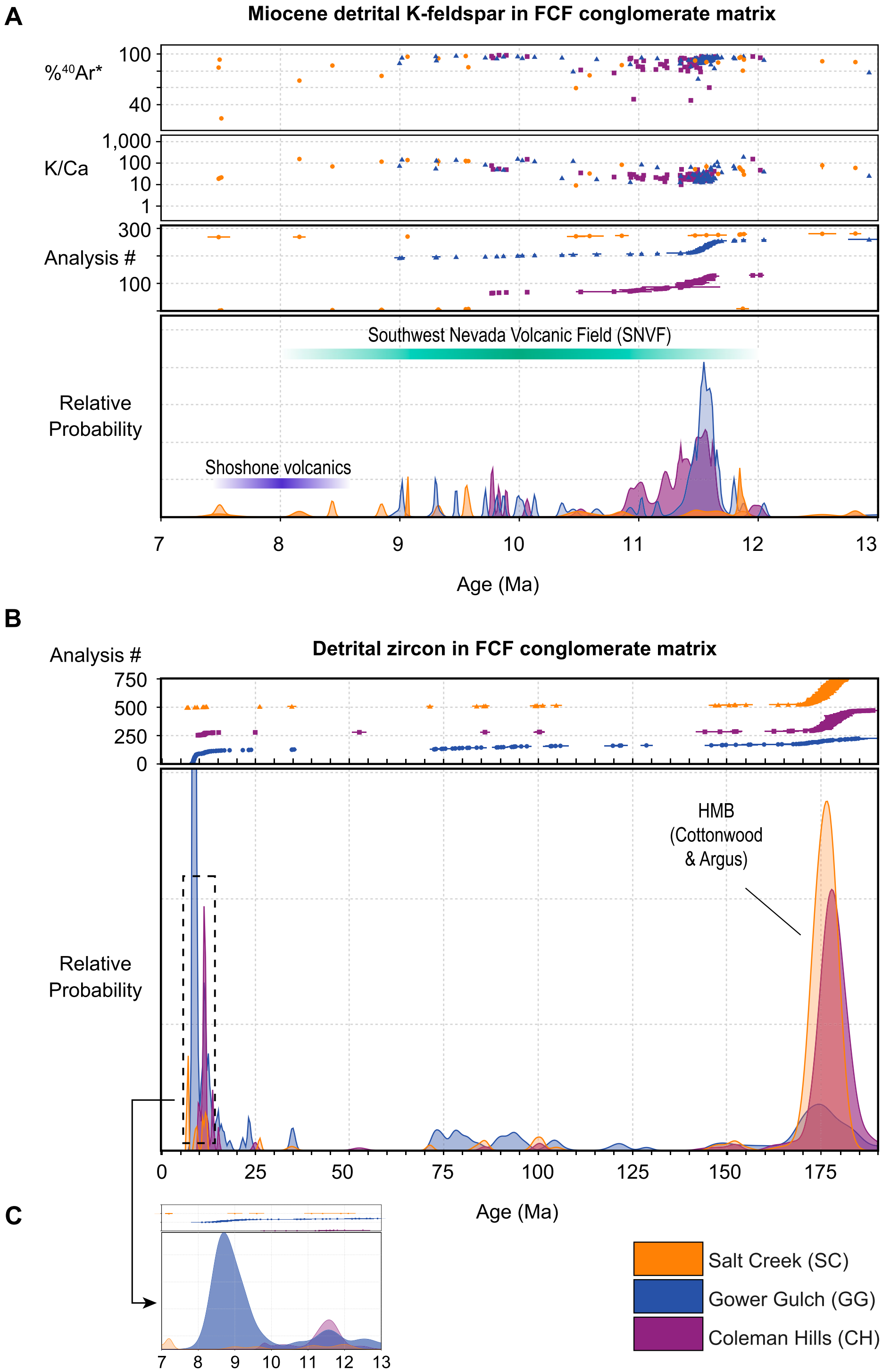

Figure 10. Age-frequency plots (ideograms) show the distribution of (A) detrital K-feldspar and (B and C) zircon dates from the matrix of conglomerates within the Furnace Creek Formation (FCF). %^{40}Ar*—radiogenic yield. See text for discussion. HMB—Hunter Mountain Batholith.

If the gravity low beneath the Saline Range represents subsurface plutons, the east-directed flow of lava through the valley north of Dry Mountain could indicate local high elevation from magma-chamber inflation during the early stages of construction of the Saline Range volcanic center.

We infer that, during the late Pliocene, the valley north of Dry Mountain drained north toward the alluvial-lacustrine Mio-Pliocene Ubehebe Basin at the northern end of the Cottonwood Mountains, which connected to the Furnace Creek Basin via Death Valley.

This inference is based on the fact that: (1) the modern valley (tributary to modern Death Valley) drains north toward the Ubehebe Basin, which was an active depocenter in latest Miocene to Pliocene times (Snow and Lux, 1999) and earlier. We deduce that the canyon would have drained north, not south, because there are no active depocenters southward except across Hunter Mountain and the southern Cottonwood Mountains; and (2) within the Ubehebe Basin, there are lake deposits, which suggests this area is down-fluvial gradient from the valley north of Dry Mountain.

The Pliocene fluvio-lacustrine system connected southeastward, in turn, to the Furnace Creek Basin (Knott et al., 2008, 2018). Together, the above constraints support the presence of a ca. 6–3.9 Ma fluvial drainage that extended from the White-Inyo Range, through the area now occupied by the Saline Range, through the valley at Dry Mountain (path M in Figs. 11, 14, and 15A and Table 2), and toward the Ubehebe Basin. At ca. 4 Ma, this drainage would have reached the widespread fluvio-lacustrine system present in Death Valley (paths Q and R in Figs. 2, 14, and 15A).

The Southern Fluvial Course

Our new age constraints on volcanic rocks in the Nova Basin and on Hunter Mountain Batholith-bearing conglomerates in the Furnace Creek Formation define a southern fluvial course in latest Miocene to Pliocene times (ca. 8.1–3.5 Ma). The southern fluvial course reached westward to at least the area of the modern Darwin Plateau in the southern Inyo Range and possibly to the Sierra Nevada. This is supported by (1) the presence of the east-sloping Inyo and Lindgren surfaces (Fig. 1; Jayko, 2009), and (2) the fact that lavas that erupted on the Darwin Plateau flowed northeast into Death Valley prior to formation of the modern-day northern Panamint Valley (Figs. 8 and 14; Hall, 1971; Burchfiel et al., 1987; Hodges et al., 1989; Coleman and Walker, 1990; Andrew and Walker, 2009; this study). Therefore, the late Miocene–Pliocene western drainage divide of proto-Death Valley was located at least as far west as the modern Darwin Plateau (Figs. 11, 14, and 15A).

The youngest of the Darwin Plateau lava flows (trachyandesite of Black Point) reached western Death Valley northwest of Tucki Mountain at 3.832 ± 0.006 Ma (KAH-BP-1 in Figs. 8 and 13). In general, both the presence of ca. 5.2–3.8 Ma lava flows sourced from the Darwin Plateau (Table 3 and see Supplemental Material) and the absence of Hunter Mountain Batholith

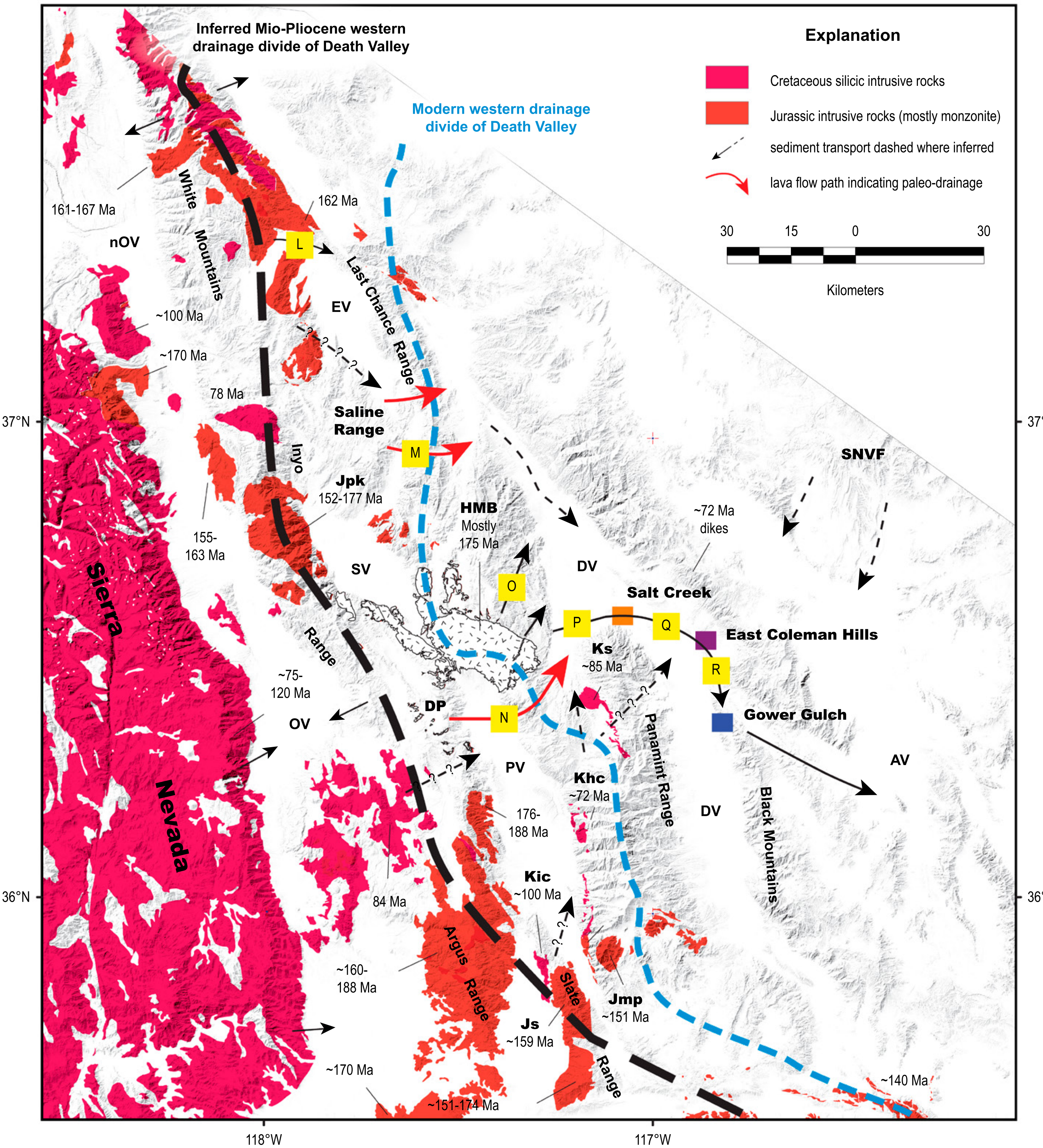

Figure 11. Map shows the distribution and ages of Jurassic and Cretaceous plutons and batholiths in the study area. The pathways with letters in yellow boxes are in Figure 2 and Table 2. Note the location of the modern (blue dashed line) versus inferred Mio-Pliocene (thick black dashed line) western drainage divide for Death Valley (DV). Mapping is from compilation of Lutz et al. (2017). Most ages are from the NAVDAT database. The following probable contributors to the age spectra in Figure 10 are shown in bold font. Kic—Isham Canyon quartz monzonite (Andrew, 2022); Ks—Skidoo granite (Barba, 2020); Khc—Hall Canyon pluton (Mahood et al., 1996); Jmp—Manly Peak quartz monzonite (Andrew, 2022); Js—Stockwell diorite (Dunne and Walker, 2004; Andrew, 2022); SNVF—Southwest Nevada Volcanic Field; AV—Amargosa Valley; EV—Eureka Valley; OV—Owens Valley; PV—Panamint Valley; SV—Saline Valley. Jpk—Jurassic Pat Keys pluton; Dp—Darwin Plateau; nOV—northern Owens Valley; HMB—Hunter Mountain Batholith.

TABLE 4. MAJOR ELEMENT COMPOSITIONS OF IGNEOUS ROCKS AND IGNEOUS ROCK CLASTS IN DEATH VALLEY REGION

Sample	Location	Latitude* (°N)	Longitude (°W)	Rock type†	Age (Ma)#	SiO_2	TiO_2	Al_2O_3	Fe_2O_3	MnO	MgO	CaO	N_2O	K_2O	P_2O_5	Total (o)
Plutonic Clasts																
EG-CWM	Cottonwood Cyn	36.64328	117.28660	MON	–	61.10	0.68	16.83	5.42	0.14	2.16	5.83	3.13	4.09	0.31	95.9
EG-GG	Gower Gulch	36.25156	116.77352	MON	177.1	64.26	0.58	15.97	4.34	0.08	1.94	4.40	3.43	4.35	0.27	91.5
EG-CH	E. Coleman Hills	36.46866	116.83814	MON	173.7	54.79	0.47	22.91	3.61	0.06	1.05	6.89	4.07	5.36	0.39	94.2
EG-SC	Salt Creek	36.60357	117.08453	MON	–	54.88	0.47	22.21	3.87	0.08	1.42	6.53	4.02	5.64	0.48	95.0
Volcanic Rocks																
Nova Basin																
KAH-BP-1	Black Point	36.54655	117.20561	BTA	3.832	56.19	1.49	15.72	6.86	0.09	4.69	8.17	3.37	2.61	0.50	91.9
KAH-TP-2	Towne Pass	36.45631	117.23982	BTA	3.904	53.26	1.50	17.19	7.40	0.14	5.58	8.47	3.66	2.04	0.45	94.0
KAH-TP-3	Towne Pass Cyn	36.36489	117.28547	TAN	3.975	56.37	1.30	18.01	6.20	0.11	4.14	6.66	4.18	2.31	0.41	94.0
KAH-PS-4	Panamint Spring	36.34579	117.49615	BAS	4.074	47.63	1.71	14.80	12.05	0.19	8.77	10.34	2.46	1.19	0.47	90.2
KAH-DP-5	Darwin Plateau	36.37963	117.59550	BAS	4.147	48.81	1.58	16.78	8.67	0.16	7.74	9.97	3.43	1.50	0.90	95.4
KAH-TP-6	Towne Pass Wash	36.34840	117.33440	TAN	4.91	57.53	1.20	17.05	6.43	0.10	3.98	6.13	4.26	2.7	0.34	88.4
KAH-AR-7	Argus Range	36.30798	117.42371	BTA	5.129	55.90	1.26	16.71	6.65	0.12	5.29	7.12	3.96	2.41	0.30	93.4
Salt Creek																
JRK-DV-1	W of Salt Creek	36.61059	117.07661	AND	4.959	58.04	1.03	15.33	6.36	0.10	5.57	6.65	3.42	2.47	0.30	95.8
Dry Mountain																
JRK-DV-3	Dry Mtn Flow	36.95202	117.57504	BAS	3.921	48.19	1.87	15.43	11.33	0.17	5.53	11.35	2.76	2.13	0.80	95.4
JRK-DV-2	Dry Mtn Cone	36.94520	117.52329	AND	4.517	61.34	0.75	15.62	5.67	0.11	3.60	5.61	3.40	3.13	0.40	94.8
Gower Gulch																
JRK-GG-1	Gower Gulch up	36.41693	116.81931	BAS	–	49.09	1.89	18.93	9.35	0.14	6.52	9.05	3.59	0.76	0.40	98.18
JRK-GG-2	Gower Gulch low	36.41697	116.81995	BAS	6.197	50.34	2.04	19.38	8.44	0.10	3.94	10.73	3.56	0.57	0.58	98.03

Notes: Data were collected by X-ray fluorescence spectrometer at Pomona College, Jonathan Harris, operator. Oxide percentages were normalized to 100% (anhydrous). Original totals are reported in last column.

*Locations are by WGS 84 datum.

†AND—Andesite; BAS—basalt; BTA—basaltic trachyandesite; MON—monazite; TAN—trachyandesite.

#See Table 3 for details regarding ages.

Cyn—Canyone; Mtn–mountain.

clasts in the Nova Basin (Hunt and Mabey, 1966; Hall, 1971; Hodges et al., 1989) support east- to northeast-directed flow from the southern Inyo Range to Death Valley during most of Pliocene time, when the Darwin Plateau lay adjacent to the Nova Basin (Fig. 15; Burchfiel et al., 1987).

The east–northeast-directed fluvial course recorded by Darwin Plateau lava flows in the Nova Basin (path N in Figs. 2, 14, and 15A) was probably connected down gradient to the Mio-Pliocene fluvial system preserved in the Furnace Creek Formation deposits at Salt Creek in Death Valley, northeast of Tucki Mountain. Hunter Mountain Batholith clasts within the middle conglomerate member of the Furnace Creek Formation at Salt Creek (path P in Figs. 11, 14, and 15A) record east- to northeastward flow from the southern Cottonwood Mountains toward Death Valley at ca. 6.9–4.96 Ma. Hunter Mountain Batholith clasts in the debris flows at East Coleman Hills (Nfcm) and Gower Gulch (Nfc) record eastward flow from the southern Cottonwood Mountains to the Furnace Creek Basin at ca. 4.1–3.5 Ma (path Q in Figs. 11, 14, and 15A) and ca. 8.1–6.2 Ma (path Q in Figs. 11, 14, and 15A), respectively.

These flow paths clearly pre-date the formation of modern Death Valley as a regional topographic low. The fluvial system recorded by these rocks certainly drained farther southeast to the modern area of Amargosa Valley during late Miocene time (e.g., Wright et al., 1999). The Miocene system may have drained yet further to the south toward the Pacific Coast, based on the paleo-geographic reconstruction in Figure 1 and Table 1. We add that crustal thickness reconstructions (Bahadori et al., 2018) and numerical simulations of paleo-topography (Zhou and Liu, 2019) support a south-facing slope between our study area (Figs. 1 and 2) and the Mojave Block.

Middle Pliocene Disconnection and Penultimate Drainage Fragmentation

Pliocene (ca. 3–5 Ma) fault-controlled topographic development and volcanism in the southwestern Great Basin fragmented the middle to late Miocene fluvial system that ran from the western highlands (White-Inyo Range) to the Furnace Creek Basin and Amargosa Valley (Figs. 14 and 15A). Destruction of the latest Miocene to Pliocene fluvial links across the southwestern Great Basin migrated east to west with tectonism, which is consistent with more regional tectonic studies (e.g., Wernicke, 1992; Snow and Wernicke, 2000; Fridrich and Thompson, 2011; Lutz et al., 2022). This migratory tectonism produced the modern system of endorheic basins (Fig. 15B).

We infer that the Miocene-aged, southeast-flowing river drainage system that connected the areas now occupied by Death Valley and Amargosa (Wright et al., 1999) was dammed and disconnected by Pliocene volcanism in the Greenwater Range (see lava flow dam in Figs. 2 and 15B). At ca. 4.0–3.9 Ma, Pliocene lavas that erupted from the Greenwater Range flowed north across the Furnace Creek Basin (Tibbetts, 2010) where the southeast-flowing braided stream system is preserved in the lower Furnace Creek Formation (Wright et al., 1999; this study). By ca. 3.5 Ma, the fluvial system was succeeded by lake sedimentation (Nfu in Fig. 14; Knott et al., 2018). The succession suggests that lava flows from the Greenwater Range dammed the pre-existing southeast-flowing river, disconnected the Furnace Creek Basin from Amargosa Valley, and promoted lake formation in the Furnace Creek Basin at ca. 3.5 Ma.

The fluvial system between the southern Cottonwood Mountains and the Furnace Creek Basin (paths Q and R in Figs. 11, 14, and 15) was broken by middle Pliocene–Holocene slip on the Black Mountains fault zone, which down-dropped modern Death Valley relative to the Black Mountains and inverted the Furnace Creek Basin (Fig. 15). Alluvial fan deposition in the northern Black Mountains, along with the angular unconformity between the Furnace Creek Formation and the overlying Funeral Formation, show that the northward expansion of the Black Mountains fault zone began at ca. 3.5 Ma and that the Furnace Creek Basin was uplifted at ca. 1.8 Ma (Knott et al., 1999, 2005). The ca. 3.5–2.8 Ma transitional member of the Furnace Creek Formation (Nft; Fig. 5) contains volcanic clasts derived from the Black Mountains (Knott et al., 2018), which further supports uplift of the range at ca. 3.5 Ma.

Thermochronometric data and modeling from the northern and central Black Mountains (Bidgoli et al., 2015; Sizemore et al., 2019) suggest 3–5 km of exhumation since ca. 4 Ma, which was achieved by slip on the Black Mountains fault zone (Figs. 2 and 15B). This is consistent

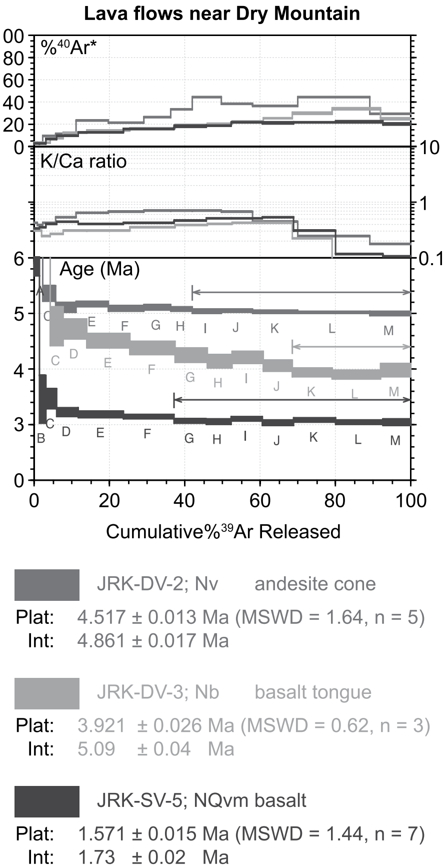

Figure 12. Age spectra from step-heating experiments performed on groundmass from lava flows in the Dry Mountain area are plotted. Eruption ages (plateaus) constrain the maximum age (andesite cone and basalt tongue) and disconnection (Saline Valley basalt) of flow through the E–W valley north of Dry Mountain (see Fig. 7). See text for discussion.

with multidisciplinary field and geochemical analyses (i.e., oxygen isotope, X-ray diffraction, and scanning electron microscope) of gouges that formed along the Black Mountains fault zone, which suggest at least 3 km of fault-zone exhumation since ca. 3 Ma (Hayman, 2006). The combination of fault-controlled uplift and basalt flows formed a topographic barrier between Death Valley and southern Amargosa Valley.

The fluvial courses that connected the Saline Range and Darwin Plateau areas to Death Valley (paths M and N in Figs. 11, 14, and 15) were fragmented by post-3.9 Ma slip on the Dry Mountain and Hunter Mountain–Panamint Valley fault zones, respectively. Slip on the kinematically linked Hunter Mountain–Panamint Valley fault zone (Fig. 8) has fragmented the southern fluvial course (Figs. 14 and 15A) by producing relief between northern Panamint Valley and the Panamint Range since ca. 3.5–4 Ma. This faulting has generated at least 1 km of relief, based on a combination of cross-sectional (Sternlof, 1988) and map-view (Burchfiel et al., 1987) reconstructions and thermochronometric modeling (Bidgoli et al., 2015). Post-3.9 Ma slip on the Dry Mountain fault zone blocked the northern fluvial course by down-dropping the Saline Range and Saline Valley relative to Dry Mountain and the rest of the southern Last Chance Range.

Slip on the Dry Mountain and Hunter Mountain–Panamint Valley fault zones produced the modern, western drainage divide at Death Valley (Panamint Range to Last Chance Range; Figs. 11 and 15), and therefore fragmented the western parts of the northern and southern fluvial courses. This fault slip took place after ca. 3.9 Ma and was likely linked kinematically with slip on the east Inyo fault zone (e.g., Burchfiel et al., 1987; Lee et al., 2009) via the Hunter Mountain fault zone (Fig. 15). We infer that this fault slip generated the modern endorheic conditions in the Panamint and Saline Valley basins (Fig. 15B), although specific evidence of internal drainage since Pliocene time was not found.

The western part of the northern fluvial course (path L in Figs. 2 and 15A) was fragmented by slip on the White Mountains and East Inyo fault zones (Figs. 1 and 2). This faulting dropped the Owens and Saline valleys down, respectively, relative to the White-Inyo Range in middle Pliocene time (Fig. 15). Sedimentological evidence (Bachman, 1978) suggests that middle Pliocene to Holocene (post-2.5 Ma) slip on these fault zones generated 1–1.5 km of relief between the White-Inyo Range and Owens Valley. This is similar to the magnitude of post-2.8 Ma exhumation in the White-Inyo Range, which was estimated independently from thermochronometry and tilt reconstructions (Stockli et al., 2003; Lee et al., 2009). Slip on the White Mountains and East Inyo fault zones coincided, in part, with west-tilting of the Sierra Nevada during slip on the Sierra Nevada frontal fault zone (Fig. 1), which has generated 1.5–2.1 km of rock uplift since ca. 5 Ma (Huber, 1981; Wakabayashi and Sawyer, 2001; Phillips, 2008; Hildreth et al., 2021).

Slip on the Sierra Nevada, White Mountains, and east Inyo fault zones created the modern Sierran crest and White-Inyo Range, which form major drainage divides in the southwestern Great Basin (Fig. 15B). The formation of Owens Valley by fault slip probably resulted in the modern, endorheic conditions within the greater Owens Valley Basin. In turn, endorheic conditions led to the drying of Pliocene lakes in Owens Valley and the formation of isolated springs (Fig. 15B). Progressive Plio-Pleistocene

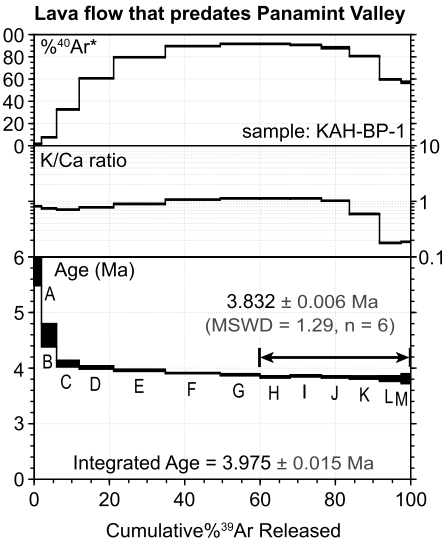

Figure 13. Age spectrum are plotted from a step-heating experiment performed on the groundmass of the trachyandesite of Black Point (KAH-BP-1), the youngest lava flow in the Nova Basin that predates the formation of northern Panamint Valley. MSWD—mean square of weighted deviates.

drying and salinization of the Owens Valley Lake system is preserved in the sedimentary (Lueddecke et al., 1998) and fossil (Oseguera, 2012) records of the ca. 2.63–2.06 Ma Waucoba Lake Beds (De Masi, 2013).

Implications for the Evolution of Endemic Species

Pliocene fault- and volcanic-controlled fragmentation of the fluvial courses described above (Fig. 15) corresponds temporally with the evolution of several endemic lineages of springsnails and pupfish that live in Owens, Death, and Amargosa valleys (ca. 2–5 Ma; e.g., Echelle, 2008; Hershler and Liu, 2008; Hershler et al., 2011, 2013). Interestingly, the endemic species have Miocene ancestors that lived in the Gila River Basin, coastal California, and northern Mexico. How the ancestral forms entered the southwestern Great Basin and what drove their subsequent divergence and endemism remains unknown. Further understanding is contingent on more robust reconstructions of early to middle Miocene paleogeography of a broader area.

Regardless of how the ancestors entered the area now occupied by the southwestern Great Basin, we hypothesize that subsequent divergent speciation was driven by Pliocene (ca. 3.5–4 Ma) geographic isolation, which was the direct consequence of both fault-controlled topographic development and local volcanism that fragmented the pre-existing fluvial network (Fig. 15). If true, then intraplate tectonics exerted

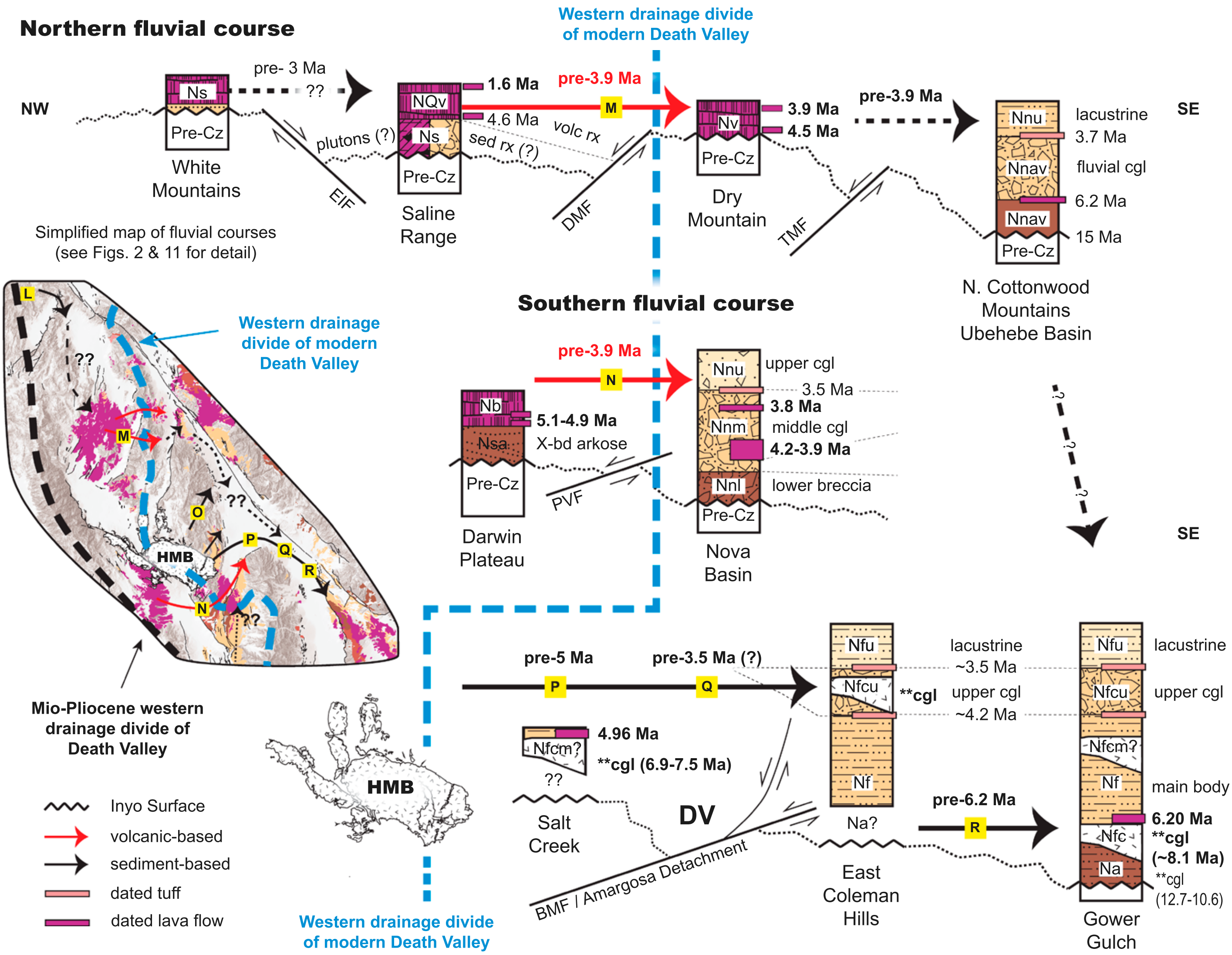

Figure 14. Stratigraphic correlation diagrams show the northern (top) and southern (bottom) fluvial courses (red and black arrows) documented in this study. Double asterisk indicates where Hunter Mountain Batholith (HMB) clasts are found in conglomerates. New dates from this study are marked in small bold text adjacent to the columns. Other dates are from Knott et al. (2018), Snow and Lux (1999), and Elliott et al. (1984). Na—Neogene Artist Drive Formation; Nf—Neogene Furnace Creek Formation; Nfc—Neogene Furnace Creek Formation Conglomerate (m-middle; u-upper); Nn (u/m/l)—Neogene Nova Formation; Nnav—Neogene Navadu Formation; Ns—Neogene sedimentary rocks; Nsa—Neogene Arkose; NQv—Neogene–Quaternary volcanic rocks; BMF—Black Mountains fault zone; DMF—Dry Mountain fault zone; DV—Death Valley; EIF—East Inyo fault zone; PVF—Panamint Valley fault zone; TMF—Tin Mountain fault zone.

first-order control on the biological evolution of endemic spring-dwelling taxa over relatively short length (<100 km) and time scales (a few millions of years). This type of tectonic control on evolutionary biology has not been demonstrated over such short spatial and temporal scales before.

Drivers of Pliocene Tectonic-Controlled Isolation

Regional middle Pliocene (ca. 3.5–4 Ma) topographic development and hydrological isolation in the southwestern Great Basin (Fig. 15) was the result of a westward migration of faulting (Wernicke, 1992; Snow and Wernicke, 2000; Fridrich and Thompson, 2011). The westward migration of intraplate faulting has been explained previously by (1) dynamic buoyancy due to return asthenospheric flow in the wake of a delaminated crustal root in the southern Sierra Nevada (Ducea and Saleeby, 1998; Farmer et al., 2002; Saleeby et al., 2003; Jones et al., 2004; Jones and Saleeby, 2013), (2) localization of range-bounding fault zones due to plate-boundary kinematic changes (e.g., Wernicke et al., 1988; Snow and Wernicke, 2000; Stockli et al., 2003; Unruh et al., 2003; McQuarrie and Wernicke 2005; Fridrich and Thompson, 2011; Walker et al., 2014; Lutz et al., 2022), and (3) internal rheological changes in the eastern Death Valley area that caused a shift in strain localization (e.g., Wernicke, 1992; Harry et al., 1993; Fridrich and Thompson, 2011; Lutz et al., 2021, 2022). Critical evaluation of these three tectonic drivers, which are not mutually exclusive, is beyond the scope of this paper.

Regardless of the driver(s), the result was a rapid change in the regional hydrological framework. Late Pliocene to Holocene tectonics and volcanism fragmented a preexisting Mio-Pliocene drainage system and created new

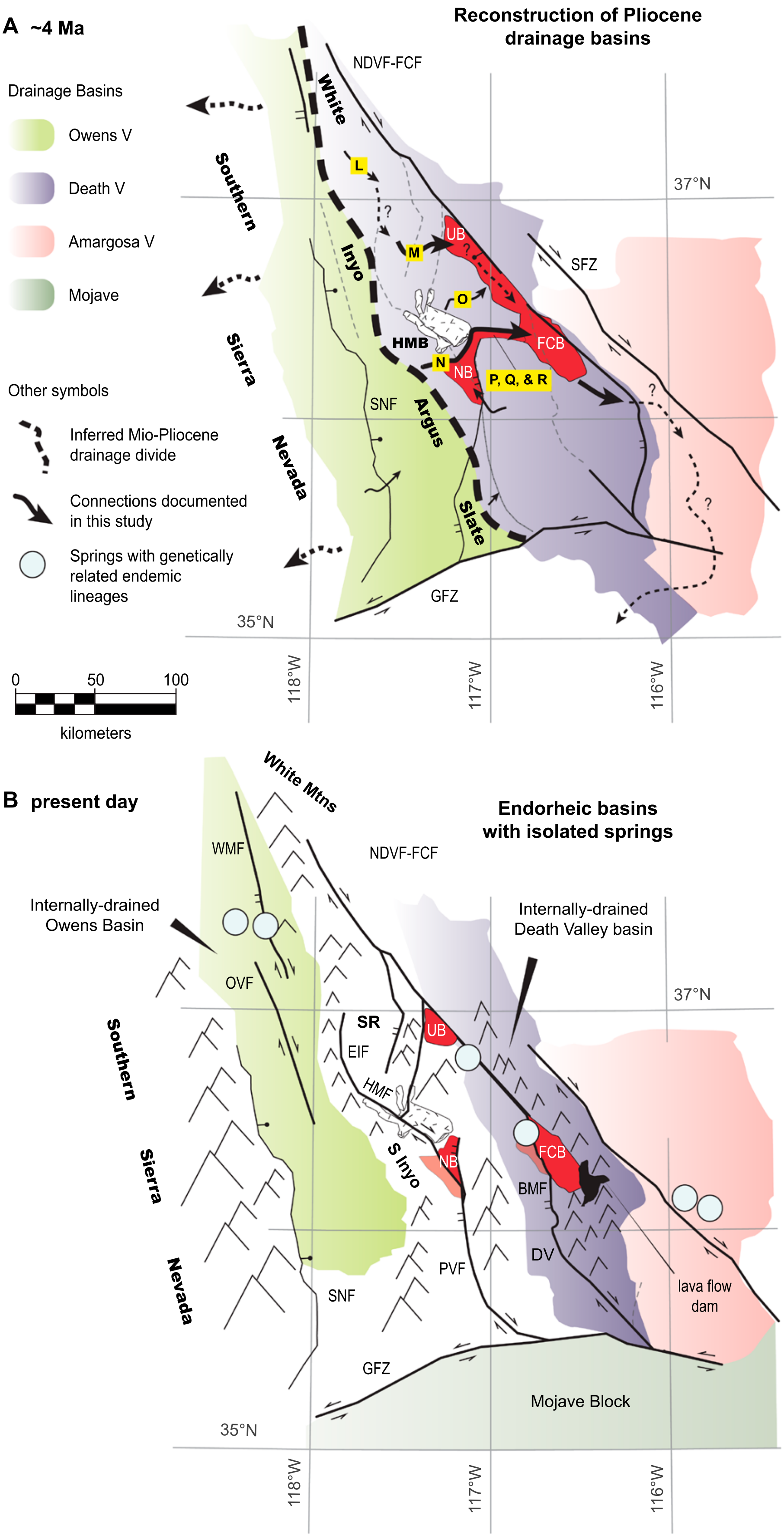

Figure 15. Map-view reconstruction shows (A) Pliocene drainage basins that predated (B) the modern, endorheic subbasins of the southwestern Great Basin. Reconstructed locations of faults in panel A are simplified from Lutz et al. (2022). Grey dashed lines in panel A are faults that accrued the most slip after ca. 4 Ma and formed much of the modern Basin and Range topography. Letters "L, M, R, etc.," refer to constraints documented in other figures and in the text. The red areas indicate the interconnected northern and southern fluvial courses. FCB—Furnace Creek Basin; NB—Nova Basin; UB—Ubehebe Basin; BMF—Black Mountains fault zone; EIF—East Inyo fault zone; GFZ—Garlock fault zone; HMB—Hunter Mountain Batholith; HMF—Hunter Mountain fault zone; NDVF–FCF—Northern Death Valley–Furnace Creek fault zone; OVF—Owens Valley fault zone; PV—Panamint Valley; SFZ—Stateline fault zone; SNF—Sierra Nevada frontal fault zone; WMF—White Mountains fault zone; DV—Death Valley; SR—Saline Range.

environmental niches over the course of 1–2 m.y. The relatively rapid tectonically controlled fragmentation isolated previously interbreeding populations of spring-dwelling taxa, which led to divergent evolution and endemism.

CONCLUSIONS

We documented the existence and subsequent fragmentation of a Mio-Pliocene drainage network in the southwestern Great Basin. Previously connected remnants of this drainage system, now preserved in ranges, are now disrupted and separated by hydrologically isolated, endorheic basins (Fig. 15B).

Our results support the existence of two interconnected drainages (or fluvial courses) that predated the local Basin and Range topography. The northern fluvial course (Figs. 14 and 15A), defined primarily by lava flows north of Dry Mountain (Fig. 7), connected the White-Inyo Range area to Death Valley between ca. 4.5 Ma and 3.8 Ma.

The southern fluvial course (Figs. 14 and 15A), represented by lava flows and alluvial fanglomerates, connected the southern Inyo Range (Darwin Plateau area) to Death Valley and Amargosa Valley in latest Miocene to Pliocene times. A connection between the southern Inyo Range and Death Valley existed before 3.8 Ma, based on lava flows in the Nova Basin.

A pre-Death Valley fluvial connection between the southern Cottonwood Mountains and the Furnace Creek Basin existed at ca. 8.1–6.2 Ma (R in Fig. 15A) based on the Hunter Mountain Batholith-bearing Conglomerate of Gower Gulch, and, speculatively, until ca. 3.5 Ma (Q in Fig. 15A), based on the conglomerate in the east Coleman Hills. Fluvial connection between the southern Cottonwood Mountains and Amargosa Valley before 8.1 Ma, and possibly as long ago as ca. 11.4 Ma, is supported by Hunter Mountain Batholith-bearing conglomerates within the Artist Drive Formation (Wright et al., 1999) and Eagle Mountain Formation (Niemi et al., 2001).

Penultimate fragmentation of the Mio-Pliocene fluvial network was achieved by transtensional, range-front faulting and local volcanism (Figs. 2 and 15). Fault-controlled topographic development was an intraplate response to one or more of three potential geodynamic drivers and formed the modern endorheic basins in the region. This rapid, tectonically controlled environmental change probably led to endemism among spring-dwelling taxa in the region through population isolation and allopatric speciation.

ACKNOWLEDGMENTS

This work was supported by National Science Foundation (NSF) Integrated Earth Systems grant EAR-1516680 (to B.M. Lutz, J.R. Knott, F.M. Phillips, and G.J. Axen) and NSF grant EAR-1649254 (to J.R. Knott). Critical reviews of the manuscript and figures by two anonymous reviewers and the associate editor greatly improved the manuscript. We are grateful to Death Valley National Park for the sampling permit. Nels Iverson, Jake Ross, Matt Zimmerer, and Levi Begay assisted with sample preparation, experimental setup, and/or data reduction at New Mexico Geochronology Laboratories. Conversations with the late Lauren Wright, Angela Jayko, Don Sada, and John Umek helped to develop this paper. We thank Mike Machette and the late Bennie Troxel for directing us toward the East Coleman Hills and Salt Creek localities. Diane Clemens-Knott, Nancy Chen, Matt Pilker, and Priscilla Martinez of California State University, Fullerton, assisted with zircon sample preparation and analysis. We also thank the staff at the University of Arizona Laserchron Center and at Pomona College for their assistance with zircon U/Pb dating and X-ray fluorescence analyses, respectively.

REFERENCES CITED

Andrew, J.E., 2010, Large-magnitude extension of the Death Valley detachment system and evolution of the Garlock fault: Geological Society of America Abstracts with Programs, v. 42, no. 4, p. 83.

Andrew, J.E., 2022, Geologic map of southern Panamint Valley, southern Panamint Range, and central Slate Range, California, USA: Geosphere, v. 18, no. 2, p. 726–727, https://doi.org/10.1130/GES02342.1.

Andrew, J.E., and Walker, J.D., 2009, Reconstructing late Cenozoic deformation in central Panamint Valley, California: Evolution of slip partitioning in the Walker Lane: Geosphere, v. 5, no. 3, p. 172–198, https://doi.org/10.1130/GES00178.1.

Antonelli, A., Kissling, W.D., Flantua, S.G., Bermúdez, M.A., Mulch, A., Muellner-Riehl, A.N., Kreft, H., Linder, H.P., Badgley, C., and Fjeldså, J., 2018, Geological and climatic influences on mountain biodiversity: Nature Geoscience, v. 11, no. 10, p. 718–725, https://doi.org/10.1038/s41561-018-0236-z.

Avila, S.T., Lackey, J.S., Lutz, B.M., Knott, J., and Mueller, N., 2018, Paleogeographic interpretation of the Fish Lake Valley/Horse Thief Hills area using geochemistry of volcanic rocks: Geological Society of America Abstracts with Programs, v. 50, no. 5, https://doi.org/10.1130/abs/2018RM-314391.

Bachman, S.B., 1978, Pliocene-Pleistocene break-up of the Sierra Nevada–White-Inyo Mountains block and formation of Owens Valley: Geology, v. 6, no. 8, p. 461–463, https://doi.org/10.1130/0091-7613(1978)6<461:PBOTSN>2.0.CO;2.

Bahadori, A., Holt, W.E., and Rasbury, E.T., 2018, Reconstruction modeling of crustal thickness and paleotopography of western North America since 36 Ma: Geosphere, v. 14, no. 3, p. 1207–1231, https://doi.org/10.1130/GES01604.1.

Barba, W.K., 2020, Tectonic evolution of the Tucki Mountain Metamorphic Core Complex, Southeastern California: Evidence for Late Cretaceous extension within the Sevier-Laramide Orogen [M.S. thesis]: Las Vegas, University of Nevada, Las Vegas, 136 p.

Barnes, H., Ekren, E.B., Rogers, C.L., and Hedlund, D.C., 1982, Geologic and tectonic maps of the Mercury quadrangle, Nye and Clark Counties, Nevada: U.S. Geological Survey Miscellaneous Investigation Series Map I-1197, scale 1:24,000.

Bidgoli, T.S., Amir, E., Walker, J.D., Stockli, D.F., Andrew, J.E., and Caskey, S.J., 2015, Low-temperature thermochronology of the Black and Panamint mountains, Death Valley, California: Implications for geodynamic controls on Cenozoic intraplate strain: Lithosphere, v. 7, no. 4, p. 473–480, https://doi.org/10.1130/L406.1.

Blakely, R.J., and McKee, E.H., 1985, Subsurface structural features of the Saline Range and adjacent regions of eastern California as interpreted from isostatic residual gravity anomalies: Geology, v. 13, no. 11, p. 781–785, https://doi.org/10.1130/0091-7613(1985)13<781:SSFOTS>2.0.CO;2.

Blakely, R.J., Jachens, R.C., Calzia, J.P., and Langenheim, V.E., 1999, Cenozoic basins of the Death Valley extended terrane as reflected in regional scale gravity anomalies, *in* Wright, L.A., and Troxel, B.W., eds., Cenozoic Basins of the Death Valley Region: Geological Society of America Special Paper 333, p. 1–16, https://doi.org/10.1130/0-8137-2333-7.1.

Brady, R.H., III, and Troxel, B.W., 1999, The Miocene Military Canyon Formation: Depocenter evolution and constraints on lateral faulting, southern Death Valley, California, *in* Wright, L.A., and Troxel, B.W., eds., Cenozoic Basins of the Death Valley Region: Geological Society of America Special Paper 333, p. 277–288, https://doi.org/10.1130/0-8137-2333-7.277.

Burchfiel, B.C., 1969, Geology of the Dry Mountain quadrangle, Inyo County, California: California Division of Mines and Geology Special Report 99, 19 p.

Burchfiel, B.C., and Stewart, J.H., 1966, "Pull-apart" origin of the central segment of Death Valley, California: Geological Society of America Bulletin, v. 77, p. 439–442, https://doi.org/10.1130/0016-7606(1966)77[439:POOTCS]2.0.CO;2.

Burchfiel, B.C., Hodges, K.V., and Royden, L.H., 1987, Geology of Panamint Valley-Saline Valley pull-apart system, California: Palinspastic evidence for low-angle geometry of a Neogene range-bounding fault: Journal of Geophysical Research: Solid Earth, v. 92, no. B10, p. 10,422–10,426, https://doi.org/10.1029/JB092iB10p10422.

Busby, C.J., and Putirka, K., 2009, Miocene evolution of the western edge of the Nevadaplano in the central and northern Sierra Nevada: Palaeocanyons, magmatism, and structure: International Geology Review, v. 51, no. 7–8, p. 670–701, https://doi.org/10.1080/00206810902978265.

Busby, C.J., Andrews, G.D.M., Koerner, A.K., Brown, S.R., Melosh, B.L., and Hagan, J.C., 2016, Progressive derangement of ancient (Mesozoic) east-west Nevadaplano paleochannels into modern (Miocene–Holocene) north–northwest trends in the Walker Lane Belt, central Sierra Nevada: Geosphere, v. 12, p. 135–175, https://doi.org/10.1130/GES01182.1.

Cassel, E.J., Breecker, D.O., Henry, C.D., Larson, T.E., and Stockli, D.F., 2014, Profile of a paleo-orogen: High topography across the present-day Basin and Range from 40 to 23 Ma: Geology, v. 42, no. 11, p. 1007–1010, https://doi.org/10.1130/G35924.1.

Çemen, I., Wright, L.A., Drake, R.E., and Johnson, F.C., 1985, Cenozoic sedimentation and sequence of deformational events at the southeastern end of Furnace Creek strike-slip fault-zone, Death Valley region, California, *in* Biddle, K.T., and Christie-Blick, N., eds., Strike-Slip Deformation, Basin Formation, and Sedimentation: Society of Economic Paleontologists and Mineralogists Special Publication 37, p. 127–139.

Çemen, I., Wright, L.A., and Prave, A.R., 1999, Stratigraphy and tectonic implications of the latest Oligocene and early Miocene sedimentary succession, southernmost Funeral Mountains, Death Valley region, California, *in* Wright, L.A., and Troxel, B.W., eds., Cenozoic Basins of the Death Valley Region: Geological Society of America Special Paper 333, p. 65–86, https://doi.org/10.1130/0-8137-2333-7.65.

Chapman, J.B., Greig, R., and Haxel, G.B., 2020, Geochemical evidence for an orogenic plateau in the southern US and northern Mexican Cordillera during the Laramide orogeny: Geology, v. 48, no. 2, p. 164–168, https://doi.org/10.1130/G47117.1.

Coleman, D.S., and Walker, J.D., 1990, Geochemistry of Mio-Pliocene volcanic rocks from around Panamint Valley, Death Valley area, California, *in* Wernicke, B.P., ed., Basin and Range Extensional Tectonics Near the Latitude of Las Vegas, Nevada: Geological Society of America Memoir 176, p. 391–412, https://doi.org/10.1130/MEM176-p391.

Coney, P.J., and Harms, T.A., 1984, Cordilleran metamorphic core complexes: Cenozoic extensional relics of Mesozoic compression: Geology, v. 12, no. 9, p. 550–554, https://doi.org/10.1130/0091-7613(1984)12<550:CMCCCE>2.0.CO;2.

Cox, B.F., Hillhouse, J.W., and Owen, L.A., 2003, Pliocene and Pleistocene evolution of the Mojave River, and associated tectonic development of the Transverse Ranges and Mojave Desert, based on borehole stratigraphy studies and mapping of landforms and sediments near Victorville, California, *in* Enzel, Y., et al., eds., Paleoenvironment and Paleohydrology of the Mojave and Southern Great Basin Deserts: Geological Society of America Special Paper 368, p. 1–42, https://doi.org/10.1130/0-8137-2368-X.1.

Craw, D., Burridge, C.P., Upton, P., Rowe, D.L., and Waters, J.M., 2008, Evolution of biological dispersal corridors through a tectonically active mountain range in New Zealand: Journal of Biogeography, v. 35, no. 10, p. 1790–1802, https://doi.org/10.1111/j.1365-2699.2008.01936.x.

DeCelles, P.G., 2004, Late Jurassic to Eocene evolution of the Cordilleran thrust belt and foreland basin system, western USA: American Journal of Science, v. 304, no. 2, p. 105–168, https://doi.org/10.2475/ajs.304.2.105.

De Masi, C.L., 2013, Ancient sedimentary fill of the Waucobi Lake Beds as an archive for Owens Valley, California tectonics and climate [M.S. thesis]: Long Beach, California State University, 93 p.

Dibblee, T.W., 1962, Displacements on the San Andreas rift zone and related structures in Carrizo Plain and vicinity, *in* Hackel, O., Geology of Carrizo Plain and San Andreas Fault: San Joaquin Geological Society, Spring Field Trip, Guidebook, p. 5–12.

Dibblee, T.W., and Minch, J.A., 2008, Geologic map of the Edison and Breckenridge Mountain 15 minute quadrangles, Kern County, California: Dibblee Geological Foundation Map DF-419, scale 1:62,500.

Dickinson, W.R., 2006, Geotectonic evolution of the Great Basin: Geosphere, v. 2, no. 7, p. 353–368, https://doi.org/10.1130/GES00054.1.

Ducea, M., and Saleeby, J., 1998, A case for delamination of the deep batholithic crust beneath the Sierra Nevada, California: International Geology Review, v. 40, no. 1, p. 78–93, https://doi.org/10.1080/00206819809465199.

Dunne, G.C., and Walker, J.D., 2004, Structure and evolution of the East Sierran thrust system, east central California: Tectonics, v. 23, https://doi.org/10.1029/2002TC001478.

Echelle, A.A., 2008, The western North American pupfish clade (*Cyprinodontidae*: Cyprinodon): Mitochondrial DNA divergence and drainage history, *in* Reheis, M.C., Hershler, R., and Miller, D.M., eds., Late Cenozoic Drainage History of the Southwestern Great Basin and Lower Colorado River Region: Geologic and Biologic Perspectives: Geological Society of America Special Paper 439, p. 27–38, https://doi.org/10.1130/2008.2439(02).

Elliott, G.S., Wrucke, C.T., and Nedell, S.S., 1984, K-Ar ages of Late Cenozoic volcanic rocks from the northern Death Valley region, California: Isochron-West, v. 40, p. 3–8.

Farmer, G.L., Glazner, A.F., and Manley, C.R., 2002, Did lithospheric delamination trigger late Cenozoic potassic volcanism in the southern Sierra Nevada, California?: Geological Society of America Bulletin, v. 114, no. 6, p. 754–768, https://doi.org/10.1130/0016-7606(2002)114<0754:DLDTLC>2.0.CO;2.

Fowler, T.K., Jr., 1992, Geology of Shadow Mountain and the Shadow Valley basin: implications for Tertiary tectonics of the eastern Mojave Desert [M.S. thesis]: Los Angeles, University of Southern California, 160 p.

Fowler, T.K., Jr., and Calzia, J.P., 1999, Kingston Range detachment fault, southeastern Death Valley region, California; relation to Tertiary deposits and reconstruction of initial dip, *in* Wright, L.A., and Troxel, B.W., eds., Cenozoic Basins of the Death Valley Region: Geological Society of America Special Paper 333, p. 245–257, https://doi.org/10.1130/0-8137-2333-7.245.

Fowler, T.K., Jr., Friedmann, S.J., Davis, G.A., and Bishop, K.M., 1995, Two-phase evolution of the Shadow Valley Basin, south-eastern California: A possible record of footwall uplift during extensional detachment faulting: Basin Research, v. 7, no. 2, p. 165–179, https://doi.org/10.1111/j.1365-2117.1995.tb00102.x.

Fridrich, C.J., and Thompson, R.A., 2011, Cenozoic tectonic reorganizations of the Death Valley region, southeast California and southwest Nevada: U.S. Geological Survey Professional Paper 1783, 36 p.

Fridrich, C.J., Thompson, R.A., Slate, J.L., Berry, M.E., and Machette, M.N., 2012, Geologic map of the southern Funeral Mountains including nearby groundwater discharge sites in Death Valley National Park, California and Nevada: U.S. Geological Survey Scientific Investigations Map 3151, scale 1:50,000, 1 sheet, 20 p. text, https://doi.org/10.3133/sim3151.

Friedmann, S.J., 1999, Sedimentology and stratigraphy of the Shadow Valley Basin, eastern Mojave Desert, California, *in* Wright, L.A., and Troxel, B.W., eds., Cenozoic basins of the Death Valley region: Geological Society of America Special Paper 333, p. 213–244, https://doi.org/10.1130/0-8137-2333-7.213.

Gehrels, G., 2014, Detrital zircon U-Pb geochronology applied to tectonics: Annual Review of Earth and Planetary Sciences, v. 42, p. 127–149, https://doi.org/10.1146/annurev-earth-050212-124012.

Gehrels, G.E., Valencia, V., and Pullen, A., 2006, Detrital zircon geochronology by laser-ablation multicollector ICPMS at the Arizona LaserChron Center, *in* Loszewski, T., and Huff, W., eds., Geochronology: Emerging Opportunities, Paleontology Society Short Course: Paleontology Society Papers, v. 11, 10 p.

Gehrels, G.E., Valencia, V., and Ruiz, J., 2008, Enhanced precision, accuracy, efficiency, and spatial resolution of U-Pb ages by laser ablation–multicollector–inductively coupled plasma–mass spectrometry: Geochemistry, Geophysics, Geosystems, v. 9, https://doi.org/10.1029/2007GC001805.

Gilbert, C.M., Christensen, M.N., Al-Rawi, Y., and Lajoie, K.R., 1968, Structural and volcanic history of Mono Basin, California–Nevada, *in* Coats, R.R., Hay, R.L., and Anderson, C.A., eds., Studies in Volcanology: Geological Society of America Memoir 116, p. 275–330, https://doi.org/10.1130/MEM116-p275.

Hall, W.E., 1971, Geology of the Panamint Butte quadrangle, Inyo County, California: U.S. Geological Survey Bulletin 1299, 66 p.

Hamilton, W., and Myers, W.B., 1966, Cenozoic tectonics of the western United States: Reviews of Geophysics, v. 4, p. 509–549, https://doi.org/10.1029/RG004i004p00509.

Harry, D.L., Sawyer, D.S., and Leeman, W.P., 1993, The mechanics of continental extension in western North America: Implications for the magmatic and structural evolution of the Great Basin: Earth and Planetary Science Letters, v. 117, no. 1–2, p. 59–71, https://doi.org/10.1016/0012-821X(93)90117-R.

Hayman, N.W., 2006, Shallow crustal fault rocks from the Black Mountain detachments, Death Valley, CA: Journal of Structural Geology, v. 28, no. 10, p. 1767–1784, https://doi.org/10.1016/j.jsg.2006.06.017.

Henry, C.D., Hinz, N.H., Faulds, J.E., Colgan, J.P., John, D.A., Brooks, E.R., Cassel, E.J., Garside, L.J., Davis, D.A., and Castor, S.B., 2012, Eocene–early Miocene paleotopography of the Sierra Nevada–Great Basin–Nevadaplano based on widespread ash-flow tuffs and paleovalleys: Geosphere, v. 8, no. 1, p. 1–27, https://doi.org/10.1130/GES00727.1.

Hershler, R., and Liu, H., 2008, Ancient vicariance and recent dispersal of springsnails (Hydrobiidae: Pyrgulopsis) in the Death Valley system, California-Nevada, *in* Reheis, M.C., Hershler, R., and Miller, D.M., eds., Late Cenozoic Drainage History of the Southwestern Great Basin and Lower Colorado River Region: Geologic and Biologic Perspectives: Geological Society of America Special Paper 439, p. 91–101, https://doi.org/10.1130/2008.2439(04).

Hershler, R., Liu, H.-P., and Landye, J.J., 2011, New species and records of springsnails (Caenogastropoda: Cochliopidae: Tryonia) from the Chihuahuan Desert (Mexico and United States), an imperiled biodiversity hotspot: Zootaxa, v. 3001, p. 1–32, https://doi.org/10.11646/zootaxa.3001.1.1.

Hershler, R., Landye, J.J., Liu, H.-P., De la Maza Benignos, M., Ornelas, P., and Carson, E.W., 2013, New species and records of Chihuahuan Desert springsnails, with a new combination for Tryonia brunei: Western North American Naturalist, v. 74, no. 1, p. 47–65, https://doi.org/10.3398/064.074.0105.

Hildreth, W., Fierstein, J., Phillips, F.M., and Calvert, A., 2021, Trachyandesite of Kennedy Table, its vent complex, and post−9.3 Ma uplift of the central Sierra Nevada: Geological Society of America Bulletin, v. 17, https://doi.org/10.1130/B36125.1.

Hodges, K.V., McKenna, L.W., Stock, J., Knapp, J., Page, L., Sternlof, K., Silverberg, D., Wüst, G., and Walker, J.D., 1989, Evolution of extensional basins and basin and range topography west of Death Valley, California: Tectonics, v. 8, no. 3, p. 453–467, https://doi.org/10.1029/TC008i003p00453.

Huber, N.K., 1981, Amount and timing of Late Cenozoic uplift and tilt of the Central Sierra Nevada, California—Evidence from the upper San Joaquin River Basin: U.S. Geological Survey Professional Paper 1197, 28 p., https://doi.org/10.3133/pp1197.

Hunt, C.B., and Mabey, D.R., 1966, Stratigraphy and structure, Death Valley, California: U.S. Geological Survey Professional Paper 494-A, 162 p.

Jayko, A.S., 2009, Deformation of the late Miocene to Pliocene Inyo Surface, eastern Sierra region, California: *in* Oldow, J.S., and Cashman, P., eds., Late Cenozoic Structure and Evolution of the Great Basin–Sierra Nevada Transition: Geological Society of America Special Paper 447, p. 313–350.

Jones, C.H., and Saleeby, J.B., 2013, Introduction: Geodynamics and consequences of lithospheric removal in the Sierra Nevada, California: Geosphere, v. 9, no. 2, p. 188–190, https://doi.org/10.1130/GES00907.1.

Jones, C.H., Farmer, G.L., and Unruh, J., 2004, Tectonics of Pliocene removal of lithosphere of the Sierra Nevada, California: Geological Society of America Bulletin, v. 116, no. 11–12, p. 1408–1422, https://doi.org/10.1130/B25397.1.

Knott, J.R., Sarna-Wojcicki, A.M., Meyer, C.E., Tinsley, J.C., III, Wells, S.G., and Wan, E., 1999, Late Cenozoic stratigraphy and tephrochronology of the western Black Mountains piedmont, Death Valley, California: Implications for the tectonic development of Death Valley, *in* Wright, L.A., and Troxel, B.W., eds, Cenozoic Basins of the Death Valley Region: Geological Society of America Special Paper 333, p. 345–366, https://doi.org/10.1130/0-8137-2333-7.345.

Knott, J.R., Sarna-Wojcicki, A., Machette, M., and Klinger, R., 2005, Upper Neogene stratigraphy and tectonics of Death Valley—a review: Earth-Science Reviews, v. 73, no. 1–4, p. 245–270, https://doi.org/10.1016/j.earscirev.2005.07.004.

Knott, J.R., Machette, M.N., Klinger, R.E., Sarna-Wojcicki, A.M., Liddicoat, J.C., Tinsley, J.C., David, B.T., and Ebbs, V.M., 2008, Reconstructing late Pliocene to middle Pleistocene Death Valley lakes and river systems as a test of pupfish (Cyprinodontidae) dispersal hypotheses, *in* Reheis, M.C., Hershler, R., and Miller, D.M., eds., Late Cenozoic Drainage History of the Southwestern Great Basin and Lower Colorado River Region: Geologic and Biotic Perspectives: Geological Society of America Special Paper 439, p. 1–26, https://doi.org/10.1130/2008.2439(01).

Knott, J.R., Machette, M.N., Wan, E., Klinger, R.E., Liddicoat, J.C., Sarna-Wojcicki, A.M., Fleck, R.J., Deino, A.L., Geissman, J.W., Slate, J.L., Wahl, D.B., Wernicke, B.P., Wells, S.G., Tinsley, J.C., III, Hathaway, J.C., and Weamer, V.M., 2018, Late Neogene–Quaternary tephrochronology, stratigraphy, and paleoclimate of Death Valley, California, USA: Geological Society of America Bulletin, v. 130, no. 7–8, p. 1231–1255, https://doi.org/10.1130/B31690.1.

Knott, J.R., Lutz, B.M., Heizler, M., Phillips, F.M., and Heitkamp, K., 2019, Tectonic reorganization in the Death Valley area at 4 Ma: Geological Society of America Abstracts with Programs, v. 51, no. 5, https://doi.org/10.1130/abs/2019AM-337840.

Kuiper, K.F., Deino, A., Hilgen, F.J., Krijgsman, W., Renne, P.R., and Wijbrans, J.R., 2008, Synchronizing the rock clocks of Earth history: Science, v. 320, p. 500–504, https://doi.org/10.1126/science.1154339.

Larson, N.W., 1979, Chronology of Late Cenozoic basaltic volcanism: The tectonic implications along a segment of the Sierra Nevada and Basin and Range Province boundary [Ph.D. thesis]: Provo, Utah, Brigham Young University, 95 p.

Lechler, A.R., Niemi, N.A., Hren, M.T., and Lohmann, K.C., 2013, Paleoelevation estimates for the northern and central proto-Basin and Range from carbonate clumped isotope thermometry: Tectonics, v. 32, no. 3, p. 295–316, https://doi.org/10.1002/tect.20016.

Lee, J., Stockli, D.F., Owen, L.A., Finkel, R.C., and Kislitsyn, R., 2009, Exhumation of the Inyo Mountains, California: Implications for the timing of extension along the western boundary of the Basin and Range Province and distribution of dextral fault slip rates across the eastern California shear zone: Tectonics, v. 28, no. 1, https://doi.org/10.1029/2008TC002295.

Luebert, F., and Muller, L.A., 2015, Effects of mountain formation and uplift on biological diversity: Frontiers in Genetics, v. 6, https://doi.org/10.3389/fgene.2015.00054.

Lueddecke, S.B., Pinter, N., and Gans, P., 1998, Plio-Pleistocene ash falls, sedimentation, and range-front faulting along the White-Inyo Mountains front, California: The Journal of Geology, v. 106, no. 4, p. 511–522, https://doi.org/10.1086/516038.

Lutz, B.M., Ketcham, R.A., Axen, G.J., Beyene, M.A., Wells, M.L., van Wijk, J.W., Stockli, D.F., and Ross, J.I., 2021, Thermo-kinematic modeling of detachment-dominated extension, northeastern Death Valley area, USA: Implications for mid-crustal thermal-rheological evolution: Tectonophysics, v. 808, https://doi.org/10.1016/j.tecto.2021.228755.

Lutz, B.M., Axen, G.A., van Wijk, J.W., and Phillips, F.M., 2022, Whole-lithosphere shear during oblique rifting: Geology, v. 50, no. 4, p. 412–416, https://doi.org/10.1130/G49603.1.

Mahood, G.A., Nibler, G.E., and Halliday, A.N., 1996, Zoning patterns and petrologic processes in peraluminous magma chambers; Hall Canyon Pluton, Panamint Range, California: Geological Society of America Bulletin, v. 108, p. 437–453, https://doi.org/10.1130/0016-7606(1996)108<0437:ZPAPPI>2.3.CO;2.

McAllister, J.F., 1970, Geology of the Furnace Creek borate area, Death Valley, Inyo County, California: California Division of Mines and Geology Map Sheet 14, scale 1:24,000, 9 p. text.

McAllister, J.F., 1971, Preliminary geologic map of the Funeral Mountains in the Ryan quadrangle, Death Valley region, Inyo County, California: U.S. Geological Survey Open-File Report, scale 1:31,680.

McQuarrie, N., and Wernicke, B.P., 2005, An animated tectonic reconstruction of southwestern North America since 36 Ma: Geosphere, v. 1, no. 3, p. 147–172, https://doi.org/10.1130/GES00016.1.

Miller, E.L., Raftrey, M.E., and Snee, J.E.L., 2022, Downhill from Austin and Ely to Las Vegas: U-Pb detrital zircon suites from the Eocene–Oligocene Titus Canyon Formation and associated strata, Death Valley, California, *in* Craddock, J.P., Malone, D.H., Foreman, B.Z., and Konstantinou, A., eds., Tectonic Evolution of the Sevier-Laramide Hinterland, Thrust Belt, and Foreland, and Postorogenic Slab Rollback (180–20 Ma): Geological Society of America Special Paper 555, p. 359–378, https://doi.org/10.1130/2021.2555(14).

Min, K., Mundil, R., Renne, P.R., and Ludwig, K.R., 2000, A test for systematic errors in ^{40}Ar/^{39}Ar geochronology through comparison with U–Pb analysis of a 1.1 Ga rhyolite: Geochimica et Cosmochimica Acta, v. 64, p. 73–98, https://doi.org/10.1016/S0016-7037(99)00204-5.

Mueller, N.J., 2019, Pliocene kinematic reorganization, fault geometry, basin evolution, and displacement budget along the Furnace Creek–Fish Lake Valley Fault Zone, eastern California and western Nevada [Ph.D. dissertation]: Dallas, Texas, University of Texas, Dallas, 161 p.

Muessig, S.J., Pennell, W.M., Knott, J.R., and Calzia, J.P., 2019, Geology of the Monte Blanco borate deposits, Furnace Creek Wash, Death Valley, California: U.S. Geological Survey Open-File Report 2019-111, 30 p., https://doi.org/10.3133/ofr20191111.

Murray, D.A., Stamatakos, J.A., and Ridgeway, K.D., 2002, Regional stratigraphy of Oligocene and lower Miocene strata in the Yucca Mountain region: San Antonio, Texas, Center for Nuclear Waste Regulatory Analyses Report, 30 p.

Niemi, N.A., 2012, Geologic map of the central Grapevine Mountains: Inyo County, California and Esmeralda and Nye Counties, Nevada: Geological Society of America Digital Map and Chart Series 12, https://10.1130/2012.DMCH012.

Niemi, N., 2013, Detrital zircon age to discriminate tectonic and fluvial transport: Geosphere, v. 9, no. 1, p. 126–137, https://doi.org/10.1130/GES00820.1.

Niemi, N.A., Wernicke, B.P., Brady, R.J., Saleeby, J.B., and Dunne, G.C., 2001, Distribution and provenance of the middle Miocene Eagle Mountain Formation, and implications for regional kinematic analysis of the Basin and Range province: Geological Society of America Bulletin, v. 113, no. 4, p. 419–442, https://doi.org/10.1130/0016-7606(2001)113<0419:DAPOTM>2.0.CO;2.

Oseguera, J.R., 2012, Ostracodes and Gastropods of the Waucobi Lake Beds: Significance for Pliocene environmental and climate conditions in the Eastern Sierra Nevada, California [M.S. thesis]: Riverside, California, University of California, Riverside, https://escholarship.org/uc/item/5m33c5 × 5.

Perrigo, A., Hoorn, C., and Antonelli, A., 2020, Why mountains matter for biodiversity: Journal of Biogeography, v. 47, no. 2, p. 315–325, https://doi.org/10.1111/jbi.13731.

Phillips, F.M., 2008, Geological and hydrological history of the paleo-Owens River drainage since the late Miocene, *in* Reheis, M.C., Hershler, R., and Miller, D.M., eds., Late Cenozoic Drainage History of the Southwestern Great Basin and Lower Colorado River Region: Geologic and Biotic Perspectives: Geological Society of America Special Paper 439, p. 115–150, https://doi.org/10.1130/2008.2439(06).

Phillips, F.M., McIntosh, and Dunbar, N.W., 2011, Chronology of late Cenozoic volcanic eruptions onto relict surfaces in the south-central Sierra Nevada, California: Geological Society of America Bulletin, v. 123, no. 5–6, p. 890–910, https://doi.org/10.1130/B30000.1.

Prave, A.R., and McMackin, M.R., 1999, Depositional framework of mid- to late Miocene strata, Dumont Hills and southern margin Kingston Range; implications for the tectonostratigraphic evolution of the southern Death Valley region, *in* Wright, L.A., and Troxel, B.W., eds., Cenozoic Basins of the Death Valley Region: Geological Society of America Special Paper 333, p. 259–275, https://doi.org/10.1130/0-8137-2333-7.259.

Rahbek, C., Borregaard, M.K., Antonelli, A., Colwell, R.K., Holt, B.G., Nogues-Bravo, D., Rasmussen, C.M.Ø., Richardson, K., Rosing, M.T., Whittaker, R.J., and Fjeldså, J., 2019, Building mountain biodiversity: Geological and evolutionary processes: Science, v. 365, no. 6458, p. 1114–1119, https://doi.org/10.1126/science.aax0151.

Reheis, M.C., and Sawyer, T.L., 1997, Late Cenozoic history and slip rates for the Fish Lake Valley, Emigrant Peak and Deep Springs fault zones, Nevada and California: Geological Society of America Bulletin, v. 109, p. 280–299, https://doi.org/10.1130/0016-7606(1997)109<0280:LCHASR>2.3.CO;2.

Renik, B., Christie-Blick, N., Troxel, B.W., Wright, L.A., and Niemi, N.A., 2008, Re-evaluation of the middle Miocene Eagle Mountain Formation and its significance as a piercing point for the interpretation of extreme extension across the Death Valley Region, California, U.S.A: Journal of Sedimentary Research, v. 78, no. 3, p. 199–219, https://doi.org/10.2110/jsr.2008.022.

Reynolds, M.W., 1969, Stratigraphy and structural geology of the Titus and Titanothere Canyons area, Death Valley, California [Ph.D. thesis]: University of California, Berkley, 310 p.

Saleeby, J., Ducea, M., and Clemens-Knott, D., 2003, Production and loss of high-density batholithic root, southern Sierra Nevada, California: Tectonics, v. 22, no. 6, https://doi.org/10.1029/2002TC001374.

Schweig, E.S., III, 1989, Basin-range tectonics in the Darwin Plateau, southwestern Great Basin, California: Geological Society of America Bulletin, v. 101, p. 652–662, https://doi.org/10.1130/0016-7606(1989)101<0652:BRTITD>2.3.CO;2.

Sizemore, T., Wielicki, M.M., Cemen, I., Stockli, D., Heizler, M., and Robinson, D., 2019, Structural evolution of central Death Valley, California, using new thermochronometry of the Badwater turtleback: Lithosphere, v. 11, no. 4, p. 436–447, https://doi.org/10.1130/L1044.1.

Snow, J.K., and Lux, D.R., 1999, Tectono-sequence stratigraphy of Tertiary rocks in the Cottonwood Mountains and northern Death Valley area, California and Nevada, *in* Wright, L.A., and Troxel, B.W., eds, Cenozoic Basins of the Death Valley Region: Geological Society of America Special Paper 333, p. 17–64, https://doi.org/10.1130/0-8137-2333-7.17.

Snow, J.K., and Wernicke, B.P., 2000, Cenozoic tectonism in the central Basin and Range; magnitude, rate, and distribution of upper crustal strain: American Journal of Science, v. 300, no. 9, p. 659–719, https://doi.org/10.2475/ajs.300.9.659.

Snyder, N.P., and Hodges, K.V., 2000, Depositional and tectonic evolution of a supradetachment basin: ^{40}Ar/^{39}Ar geochronology of the Nova Formation, Panamint Range, California: Basin Research, v. 12, no. 1, p. 19–30, https://doi.org/10.1046/j.1365-2117.2000.00108.x.

Spencer, J.E., 1990, Late Cenozoic extensional and compressional tectonism in the southern and western Avawatz Mountains, southeastern California, *in* Wernicke, B., ed., Basin and Range Extensional Tectonics near the Latitude of Las Vegas, Nevada: Geological Society of America Memoir 176, p. 317–333, https://doi.org/10.1130/MEM176-p317.

Steiger, R.H., and Jäger, E., 1977, Subcommission on geochronology: Convention on the use of decay constants in geo- and cosmochronology: Earth and Planetary Science Letters, v. 36, p. 359–362, https://doi.org/10.1016/0012-821X(77)90060-7.

Sternlof, K.R., 1988, Structural style and kinematic history of the active Panamint-Saline extensional system, Inyo county, California [Ph.D. thesis]: Cambridge, Massachusetts Institute of Technology, 30 p.

Stewart, J.H., 1967, Possible large right-lateral displacement along fault and shear zones in the Death Valley–Las Vegas area, California and Nevada: Geological Society of America Bulletin, v. 78, no. 2, p. 131–142, https://doi.org/10.1130/0016-7606(1967)78[131:PLRDAF]2.0.CO;2.

Stewart, J.H., 1983, Extensional tectonics in the Death Valley area, California: Transport of the Panamint Range structural block 80 km northwestward: Geology, v. 11, no. 3, p. 153–157, https://doi.org/10.1130/0091-7613(1983)11<153:ETITDV>2.0.CO;2.

Stockli, D.F., Dumitru, T.A., McWilliams, M.O., and Farley, K.A., 2003, Cenozoic tectonic evolution of the White Mountains, California and Nevada: Geological Society of America Bulletin, v. 115, no. 7, p. 788–816, https://doi.org/10.1130/0016-7606(2003)115<0788:CTEOTW>2.0.CO;2.

Tibbetts, A.K., 2010, Petrogenesis of the Greenwater Range: Comparison to the Crater Flat volcanic field and implications for hazard assessment [M.S. thesis]: Las Vegas, Nevada, University of Nevada, Las Vegas, 150 p., https://doi.org/10.34917/1436699.

Unruh, J., Humphrey, J., and Barron, A., 2003, Transtensional model for the Sierra Nevada frontal fault system, eastern California: Geology, v. 31, no. 4, p. 327–330, https://doi.org/10.1130/0091-7613(2003)031<0327:TMFTSN>2.0.CO;2.

Wakabayashi, J., and Sawyer, T.L., 2001, Stream incision, tectonics, uplift, and evolution of topography of the Sierra Nevada, California: The Journal of Geology, v. 109, no. 5, p. 539–562, https://doi.org/10.1086/321962.

Walker, J.D., Bidgoli, T.S., Didericksen, B.D., Stockli, D.F., and Andrew, J.E., 2014, Middle Miocene to recent exhumation of the Slate Range, eastern California, and implications for the timing of extension and the transition to transtension: Geosphere, v. 10, no. 2, p. 276–291, https://doi.org/10.1130/GES00947.1.

Wernicke, B., 1992, Cenozoic extensional tectonics of the U.S. Cordillera, *in* Burchfiel, B.C., Lipman, P.W., and Zoback, M.L., eds., The Cordilleran Orogen: Conterminous U.S.: Boulder, Colorado, Geologic Society of America, The Geology of North America, v. G-3, p. 553–581, https://doi.org/10.1130/DNAG-GNA-G3.553.

Wernicke, B.P., Axen, G.J., and Snow, J.K., 1988, Basin and Range extensional tectonics at the latitude of Las Vegas, Nevada: Geological Society of America Bulletin, v. 100, no. 11, p. 1738–1757, https://doi.org/10.1130/0016-7606(1988)100<1738:BARETA>2.3.CO;2.

Workman, J.B., Menges, C., Fridrich, C.J., and Thompson, R.A., 2016, Geologic map of Death Valley National Park, Nevada and California: Geological Society of America Abstracts with Programs, v. 48, no. 7, https://doi.org/10.1130/abs/2016AM-286651.

Wright, L.A., and Troxel, B.W., 1993, Geologic map of the central and northern Funeral Mountains and adjacent areas, Death Valley region, southern California: U.S. Geological Survey Miscellaneous Investigations Map 2305, 1:48,000.

Wright, L.A., Otton, J.K., and Troxel, B.W., 1974, Turtleback surfaces of Death Valley viewed as phenomena of extensional tectonics: Geology, v. 2, no. 2, p. 53–54, https://doi.org/10.1130/0091-7613(1974)2<53:TSODVV>2.0.CO;2.

Wright, L.A., Greene, R.C., Cemen, I., Johnson, F.C., and Prave, A.R., 1999, Tectonostratigraphic development of the Miocene–Pliocene Furnace Creek Basin and related features, Death Valley region, California, *in* Wright, L.A., and Troxel, B.W., eds., Cenozoic Basins of the Death Valley Region: Geological Society of America Special Paper 333, p. 87–114, https://doi.org/10.1130/0-8137-2333-7.87.

Wrucke, C.T., and Corbett, K.P., 1990, Geologic map of the Last Chance quadrangle, California and Nevada: U.S. Geological Survey Open-File Report 90–647-A, scale 1:62,500.

Zhou, Q., and Liu, L., 2019, Topographic evolution of the western United States since the early Miocene: Earth and Planetary Science Letters, v. 514, p. 1–12, https://doi.org/10.1016/j.epsl.2019.02.029.

Science Editor: Brad Singer
Associate Editor: Michael Smith

Manuscript Received 16 October 2021
Revised Manuscript Received 31 August 2022
Manuscript Accepted 28 September 2022

Printed in the USA